REPORT DOCUMENTATION PAGE		Form Approved OMB No. 0704-0188

1. REPORT DATE *(DD-MM-YYYY)* 08-09-2010	2. REPORT TYPE Final Report	3. DATES COVERED *(From – To)* 4 September 2009 - 04-Sep-10

4. TITLE AND SUBTITLE

Scaled-Up Nonequilibrium Air Plasmas

5a. CONTRACT NUMBER
FA8655-09-1-3110

5b. GRANT NUMBER

5c. PROGRAM ELEMENT NUMBER

6. AUTHOR(S)

Dr. Zdenko Machala

5d. PROJECT NUMBER

5d. TASK NUMBER

5e. WORK UNIT NUMBER

7. PERFORMING ORGANIZATION NAME(S) AND ADDRESS(ES)
Comenius University
FMFI UK
Bratislava 84248
SLOVAKIA

8. PERFORMING ORGANIZATION REPORT NUMBER

N/A

9. SPONSORING/MONITORING AGENCY NAME(S) AND ADDRESS(ES)

EOARD
Unit 4515 BOX 14
APO AE 09421

10. SPONSOR/MONITOR'S ACRONYM(S)

11. SPONSOR/MONITOR'S REPORT NUMBER(S)
Grant 09-3110

12. DISTRIBUTION/AVAILABILITY STATEMENT

Approved for public release; distribution is unlimited.

13. SUPPLEMENTARY NOTES

14. ABSTRACT

The objective of the current program is to investigate the volume scalability of nonequilibrium plasmas produced by electrical discharges in atmospheric pressure air. Both DC and repetitively pulsed discharges have been successfully demonstrated to form non-equilibrium air plasmas at atmospheric pressure with temperatures below 2000 K and electron densities above 10_{12} cm$_{-3}$. Such plasmas represent a potential for aircraft shielding, and many other applications, e.g. biodecontamination. The critical issues are the dimensions of these plasma discharges that are typically limited to cm-lengths and mm-diameters at maximum, and the power requirements.

Key results demonstrate that both DC glow discharge and pulsed transient spark generate air plasmas of required parameters. Glow discharge is easier for volume scaling but requires larger power. Glow discharge operated in fast air flows preheated to 2000 K improves the volume scaling but at very high powers (including the preheating). The preheated air can be set below 2000 K at slower flows, thus enabling partial gas heating of the discharge. Corona discharge as a temperature probe was developed to diagnose the microwave torch preheated air.

A new concept of the DC-driven pulsed discharge was tested: *transient spark (TS)*, a repetitive streamer-to-spark transition discharge regime of very short pulse duration (~10-100 ns) and with a very limited

energy so that the generated plasma is highly nonequilibrium. This discharge can be maintained at low energy conditions by an appropriate choice of the resistances and capacities in the electrical circuit, and its frequency can be controlled by the applied voltage. Its activity is comparable with the nanosecond repetitive pulsed discharges but its advantage is an ease of the DC operation and no need of special and expensive high voltage pulsers with high repetitive frequency and nanosecond rise-times. Our calculations of temporal evolution of electron density in TS based on detailed analysis of the electrical circuit show that $\sim 10^{16}$ cm$_{-3}$ at maximum and $\sim 10^{11}$ cm$_{-3}$ in average are reached. By setting the parameters of the electric circuit (resistances, capacity) it is possible to control the TS parameters and properties.

Time-integrated and temporally-resolved optical emission spectroscopy combined with electrical measurements are used as principal discharge diagnostics techniques. Investigating the processes occurring during TS pulse evolution on nanosecond time scales is crucial for deeper understanding of its chemical and physical activity. Transient spark was also studied in preheated air flows. Preheated air decreases the gas density and simulates lowered pressure, which is generally favorable for plasma scaling and high altitude aircraft shielding. Applying TS in preheated air is also interesting for the tests of lean flame stabilization. New interesting phenomena and transitions between streamer-spark-glow discharge regimes were revealed as function of input gas temperature.

15. SUBJECT TERMS
EOARD, Plasma Physics

16. SECURITY CLASSIFICATION OF:			17. LIMITATION OF ABSTRACT	18, NUMBER OF PAGES	19a. NAME OF RESPONSIBLE PERSON
a. REPORT UNCLAS	**b. ABSTRACT** UNCLAS	**c. THIS PAGE** UNCLAS	UL	56	Brad Thompson
					19b. TELEPHONE NUMBER *(Include area code)* +44 (0)1895 616163

SCALED-UP NONEQUILIBRIUM AIR PLASMAS GENERATED BY DC AND PULSED DISCHARGES

Comprehensive Final Report

for the period: 4 September 2009 – 3 September 2010

Submitted to

Dr. Brad Thompson

European Office of Aerospace Research and Development

Air Force Office of Scientific Research

Grant No. FA8655-09-1-3110

Submitted by

Professor Zdenko Machala (Principal Investigator)

Department of Astronomy, Earth Physics and Meteorology

Faculty of Mathematics, Physics and Informatics, Comenius University

Mlynska dolina F2, 84248 Bratislava, Slovakia

tel: +421-2-60295618, fax: +421-2-65425982

email: machala@fmph.uniba.sk

http://enviro.fmph.uniba.sk/machala

September 2010

Contents

List of Figures

1. Abstract

The objective of the current program is to investigate the volume scalability of nonequilibrium plasmas produced by electrical discharges in atmospheric pressure air. Both DC and repetitively pulsed discharges have been successfully demonstrated to form non-equilibrium air plasmas at atmospheric pressure with temperatures below 2000 K and electron densities above 10^{12} cm^{-3}. Such plasmas represent a potential for aircraft shielding, and many other applications, e.g. bio-decontamination. The critical issues are the dimensions of these plasma discharges that are typically limited to cm-lengths and mm-diameters at maximum, and the power requirements.

Key results demonstrate that both DC glow discharge and pulsed transient spark generate air plasmas of required parameters. Glow discharge is easier for volume scaling but requires larger power. Glow discharge operated in fast air flows preheated to 2000 K improves the volume scaling but at very high powers (including the preheating). The preheated air can be set below 2000 K at slower flows, thus enabling partial gas heating of the discharge. Corona discharge as a temperature probe was developed to diagnose the microwave torch preheated air.

A new concept of the DC-driven pulsed discharge was tested: *transient spark (TS)*, a repetitive streamer-to-spark transition discharge regime of very short pulse duration (~10-100 ns) and with a very limited energy so that the generated plasma is highly nonequilibrium. This discharge can be maintained at low energy conditions by an appropriate choice of the resistances and capacities in the electrical circuit, and its frequency can be controlled by the applied voltage. Its activity is comparable with the nanosecond repetitive pulsed discharges but its advantage is an ease of the DC operation and no need of special and expensive high voltage pulsers with high repetitive frequency and nanosecond rise-times. Our calculations of temporal evolution of electron density in TS based on detailed analysis of the electrical circuit show that ~10^{16} cm^{-3} at maximum and ~10^{11} cm^{-3} in average are reached. By setting the parameters of the electric circuit (resistances, capacity) it is possible to control the TS parameters and properties.

Time-integrated and temporally-resolved optical emission spectroscopy combined with electrical measurements are used as principal discharge diagnostics techniques. Investigating the processes occurring during TS pulse evolution on nanosecond time scales is crucial for deeper understanding of its chemical and physical activity. Transient spark was also studied in preheated air flows. Preheated air decreases the gas density and simulates lowered pressure, which is generally favorable for plasma scaling and high altitude aircraft shielding. Applying TS in preheated air is also interesting for the tests of lean flame stabilization. New interesting phenomena and transitions between streamer-spark-glow discharge regimes were revealed as function of input gas temperature.

2. Introduction

This annual report describes progress on our research program "Scaled-up Nonequilibrium Air Plasmas Generated by DC and Pulsed Discharges." This program is supported by a grant from the European Office of Aerospace Research and Development of Air Force Office of Scientific Research (Grant No. FA8655-09-1-3110) and is conducted in the group of Prof. Zdenko Machala at Comenius University in Bratislava. This research program is tightly linked to the previous EOARD AFOSR research program (Grant No. FA8655-08-1-3061) and follows up the results obtained by the Stanford Consortium of the Plasma Rampart MURI program (Mechanisms of Ionizational Nonequilibrium in Air Plasmas, 1997-2002), and by the Stanford University program (Scaled-Up Nonequilibrium Air Plasmas, 2001-2004), both financed by AFOSR. Prof. Zdenko Machala was personally involved in these Stanford programs in 2002-2004.

Large-volume air plasmas at atmospheric pressure present considerable interest for a wide range of Air Force applications in plasma aerodynamics and flow control. Desirable conditions are electron densities of the order of 10^{12} cm^{-3} and gas temperatures less than 2000 K. Considerable advances have been achieved in the preceding AFOSR programs (MURI program on Air Plasma Ramparts [1] and Scaled-Up Air Plasmas [2]). In particular, they have demonstrated that it is possible to produce over 10^{12} electrons/cm^3 in atmospheric pressure air with either DC or repetitively pulsed discharges. Furthermore, they have experimentally demonstrated that it takes only 12 W/cm^3 of power to produce 10^{12} electrons/cm^3 with a repetitively pulsed discharge in air. This power level is about 250 times lower than for a DC discharge producing the same electron density.

The present program seeks to expand on the results of these preceding programs. Specifically, we are interested in scaling up the DC discharges to produce larger volumes of nonequilibrium air plasma and to reduce the power budget. At the same time we make efforts to understand the elementary processes and their temporal evolution and the physical mechanisms that limit the size of an individual discharge. Nanosecond-temporal resolution of the evolution of the radiative species and the processes occurring in the pulsed transient spark leads to deeper understanding of the elementary plasma processes and active species required for multiple applications.

3. Experimental set-up, methods and results

The experimental set-up and methods used have been described in detial in the previous final report [3] (Grant No. FA8655-08-1-3061). In this program we planned buying a new high voltage pulse generator with nanosecond rise time pulses and ~10 kHz frequency range for ns pulsed discharge to be compared with DC-supplied pulsed discharge (transient spark). The ns pulsed discharges have been previously demonstrated to require about 100x less total power than DC glow discharges [2]. Unfortunately, due to a delay of grant payments and increased prices of such pulse generators on the market, we had to postpone its purchase to the next grant period. Nevertheless, we focused on deeper investigations of DC-driven transient spark discharge in ambient as well as preheated air, including developing a kinetic model.

3.1. Optical Diagnostics

Optical emission spectroscopy (OES) is known to be a very useful diagnostic technique of plasmas because it allows identification of active species and radicals in the plasma; measuring the gas temperature (as the rotational temperature T_r that equilibrates with the gas temperature owing to fast collisional relaxation at atmospheric pressure); determining the level of nonequilibrium (by comparing rotational and vibrational T_v temperatures), and under certain assumptions measuring the discharge dimensions. The OES diagnostics system was also described in the previous report. Besides using a dual fiber-optic compact spectrometer Ocean Optics SD2000 with CCD detector for fast but low resolution scanning in the UV and VIS-NIR regions (200-500 and 500-1050 nm) we started alternatively using a 2-m monochromator Carl Zeiss Jena PGS2, covering UV and VIS (200-800 nm) and providing spectral resolution of 0.1 nm, equipped with an intensified CCD camera Andor Istar for much better spectral and temporal resolution necessary to track the nanosecond-short time scale processes occurring in the transient spark pulses.

We have described a problem with ICCD camera ns-time resolved evolutions of species in transient spark. Since the transient spark is a self-pulsing discharge, the only way to catch the pulse evolution by the ICCD camera is triggering the camera by the discharge pulse itself. However, due to the camera's insertion delay we could only get the evolution of processes and radiative species starting ~20 ns after the origin of the current pulse. Unluckily, the first 20-25 ns of the pulse are critical for N_2 second positive system which is very important for plasma temperature measurements. We are addressing this problem by using a long (10 m) optic fiber that delays the light from the discharge by more than 30 ns so that this light enters the camera after it is already triggered and ready to acquire. We adjusted our optical system to this new component.

In addition, triggering the ICCD camera by the discharge pulse itself is dangerous because it can damage the sensitive electronics in the camera if the pulse accidentally exceeds the allowed limit. So we constructed a special trigger pulse generator for the camera. The optimum trigger pulse is induced by the discharge current pulse regardless to its amplitude. This trigger pulse generator was constructed using fast transistors to keep the delay of the discharge signal to the camera system minimal (~6 ns).

In addition to nanosecond-resolved emission spectroscopy performed by the ICCD camera system, we are using photomultiplier tube (PMT) combined with wavelength-specific optical filters system to measure the nanosecond evolution of species. The PMT optical system has been set-up and the first data were obtained.

3.2. Microwave Plasma Torch

Experiments with DC discharges were planned in ambient and preheated air at atmospheric pressure. We originally preheated air to about 2000 K with a microwave plasma torch Litmas Red powered by a 5 kW magnetron Richardson Electronics switching power generator Model SM1050. The torch had a maximum power output of 3 kW. The temperature and velocity of the outgoing plasma can be set by varying the power output and gas flow rate, as well as by using water-cooled test sections and nozzles. The torch is able to generate air plasmas in the temperature range 750-4700 K at flow velocities from 20 to 1400 m/s, corresponding to gas flow rates from 8 to 110 slpm (standard liters per minute). The microwave torch head and a close-up view of the air plasma plume at typical experimental conditions were shown in the previous report [3].

Since we encountered problems with the 5 kW magnetrons (several of them have consecutively broken due to the reflected microwaves), the fragile 5 kW magnetron was therefore replaced with the sturdy 1 kW magnetron typically used in the microwave ovens which is more resistant to the reflected waves. This provides substantially lower power into the plasma, for it is only 1 kW, and is not optimally matched for our torch system, also the efficiency of the magnetron is relatively low (<50%). Nevertheless, as was shown in the previous report, even this lower power magnetron can be well used to preheat air flows up to 1500 K, which is sufficient for our investigations. On top of that, the power budget of the entire system was thus lowered. The new magnetron and its output microwave power and the reflected power were calibrated, as described in the previous report.

3.2.1. Corona as a temperature probe in the preheated air

The microwave plasma temperature can be determined by OES method by comparing the measured and simulated emission spectra. This method is very convenient but sometimes overestimates the temperature if determined from the emission spectra of radicals (e.g. CN, NO, OH). The radicals can gain energy in the chemical process of their production, which can contribute to the elevated temperature. This phenomenon was observed by other authors [4], as well as our previous investigations [5]. Therefore we determine the temperature of the plasma generated in air from N_2 spectrum only, since N_2 molecules are present in the feeding gas and are not produced by chemical processes in the plasma. In near-equilibrium MW plasma generated in air, however, the excitation of N_2 takes place at the temperatures above 6000 K [6]. Such high temperatures are hardly reached in our plasma, especially not at low power (362 W). As a consequence, there is no emission of N_2 in air. At higher powers we just observe the emission of NO and OH radicals and weak noisy O_2, so there exists no appropriate radiation for a reliable OES diagnostics. The emission spectra of the low power (362 W, 8 slpm) MW air plasma shown in Figure 1 demonstrate but the continuum radiation.

On the other hand, it is known that N_2^* is produced in non-equilibrium air plasmas, e.g. in the corona discharge. In this strongly nonequilibrium discharge, the gas temperature is low (almost room temperature) but the high temperature of electrons is sufficient for the excitation of N_2. In the

discharges at atmospheric pressure, the rotational temperature balances with the temperature of the surrounding gas. So if we put a needle electrode with DC corona discharge directly into the MW plasma (Figure 2), N_2^* is produced by electron excitation but its rotational temperature is balanced with the surrounding gas temperature – in our case, the temperature of the MW air plasma. The cold corona discharge does not significantly contribute to the increase of the gas temperature. So, by combining the MW plasma with corona, we can determine the temperature of the MW plasma (as a rotational temperature of N_2^*).
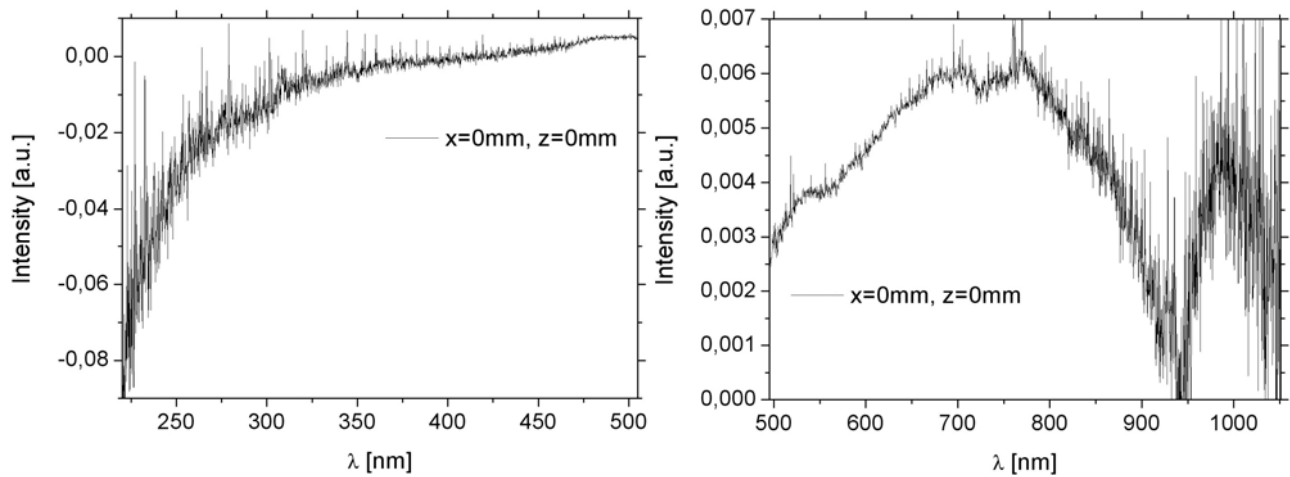
Figure 1. *UV and VIS emission spectra of the MW air plasma (362 W, 8 slpm).*
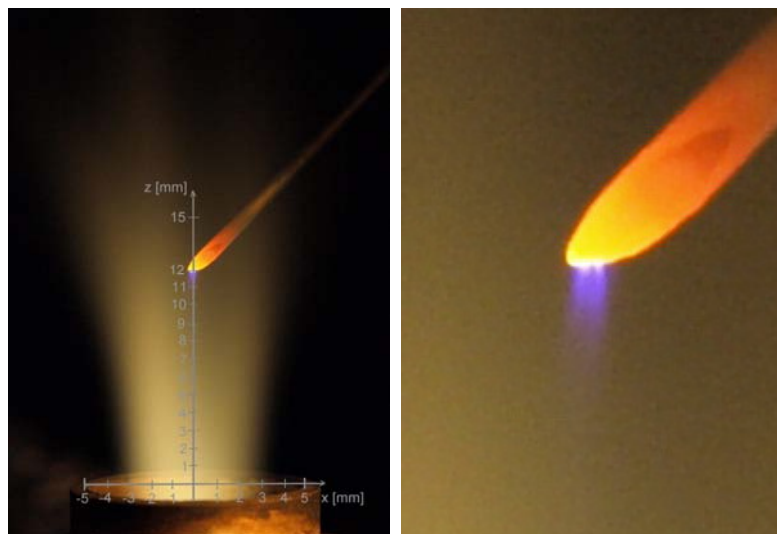
Figure 2. *Positive DC corona discharge in the MW air plasma, with indicated dimensions (left) and a detail (right).*

The typical OES spectra of a positive DC corona discharge (5 kV) in the MW preheated air (362 W, 8 slpm) are shown in Figure 3. A very distinct N_2 ($C^3\Pi_u$-$B^3\Pi_g$) system applicable for temperature measurements was detected in the UV, with the strongest intensity at 337 nm (0-0 vibrational band).

In the experiments with DC discharges in preheated air flows it is very important to know the temperature of the air flow. So we performed a series of experiments to verify this novel corona probe method of measuring the MW preheated air plasma temperature. The temperatures of the same MW air plasma jets were measured by a thermocouple, in addition to the corona probe method. The comparison of the measured temperatures by both methods is shown in Figure 4.

We observe a fairly good agreement between the MW air plasma temperatures measured by the corona probe and the thermocouple. The great advantage of our novel corona probe diagnostics method is that it can be applied up to much higher temperatures where the use of thermocouples is limited or impossible.

A journal publication of this novel diagnostics method has been submitted to *Plasma Sources Science and Technology* and is in the review process.
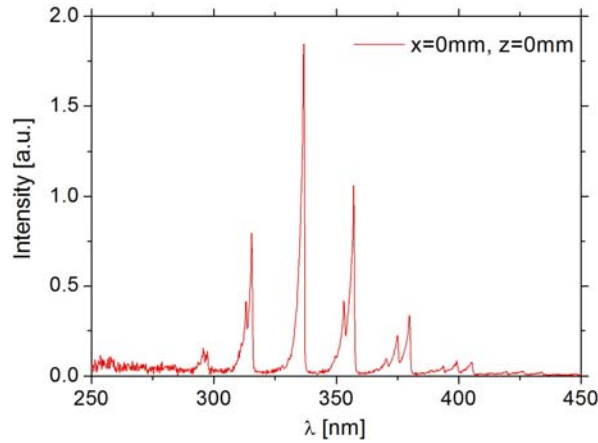
Figure 3. Typical UV emission spectra of the positive DC corona (5 kV) in the MW air plasma (362 W, 8 slpm).

Figure 4. Temperature profiles of the MW air plasma at various powers and flow rates measured by the corona probe and thermocouple. Corona 1 and 2 correspond to two measurement sets.

3.3. Transient spark (TS)

TS, depicted in Figure 5 and described in many details in the previous report [3], represents a simple solution to generate short (~100 ns) high current pulses (~1 A) with high repetition frequency f (~kHz). Simple means that TS pulses are generated by a simple and relatively cheap DC power supply. Emission spectroscopy proved tha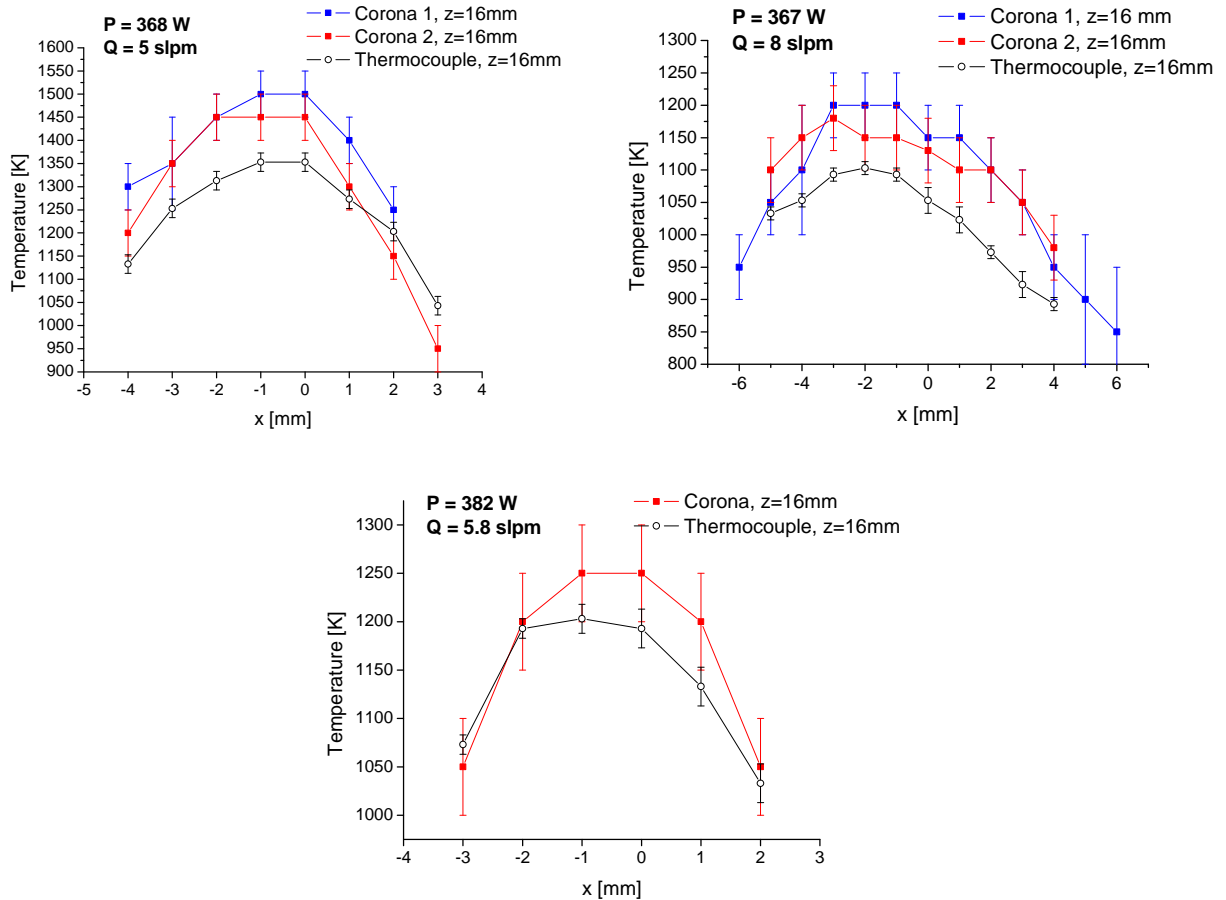t TS current pulses generate highly reactive plasma with excited atomic radicals (O*, N*) and even excited ions N_2^+*. TS has already been successfully applied for various environmental and bio-medical applications [7-9]. Various applications have different demands on TS with respect to the optimal frequency, energy per pulse, etc. So the optimization of TS for various applications requires further research.

Figure 5. Photograph of TS in positive needle – plane gap of 6 mm, aperture f/4.8. TS: 1.2 kHz, I_{max}=4 A, U=7.5 kV, R=3.5 MΩ, exposure ¼ s, ISO 200.

3.3.1. Electrical characteristics of TS

A control of the TS parameters, such as repetition frequency f, peak current in the TS pulse I_{max}, pulse duration, energy deposited to plasma per pulse, etc., is necessary to perform the optimization of TS towards various applications. These parameters can be controlled by modifying the external circuit. We performed s detailed study of the influence of external circuit parameters on TS behavior. Besides external the ballast resistor R and the internal capacity C of the system, we studied the role of an additional separating resistor r, placed between high voltage (HV) electrode and HV cable connecting it to the power supply (Figure 6). We also built a mathematical description of TS parameters dependences on these external components. Thanks to the experimental results and derived analytical expressions we are able to estimate a time evolution of the electron density n_e for various discharge regimes, including the influence of r on n_e. Detailed description of the obtained results was submitted to the journal *Plasma Sources Science and Technology* and is currently in the review process. This article is shown in full as Appendix 1.

Briefly, we showed that TS can be maintained at low energy conditions (up to 1 mJ/pulse) by an appropriate choice of the resistances and capacities in the electrical circuit, and its frequency can be controlled by the applied voltage. The activity of TS is comparable with the nanosecond repetitive pulsed discharges [10-11] but its advantage is an ease of the DC operation and no need of special and expensive high voltage pulsers with high repetitive frequency and nanosecond rise-times.

Our calculations of temporal evolution of electron density in TS based on the detailed analysis of the electrical circuit showed that $n_e \approx 10^{16}$ cm^{-3} at maximum and ~10^{11} cm^{-3} in average are reached.

We found that the increasing r causes that it takes much longer to discharge the charge stored in the HV cable and the tail of the current pulse can be thus longer than several tens of µs. This additional resistor r enables to merge the characteristics of TS and the glow discharge together, i. e. relatively high current pulses (~1 A) with a high efficiency of radical production are followed by long periods with the current above 1 mA during which plasma reaches characteristics typical for high pressure glow discharge. Our further research in this area will be focused on scaling up the TS discharge to produce larger volumes of non-equilibrium air plasma and to reduce the power budget.
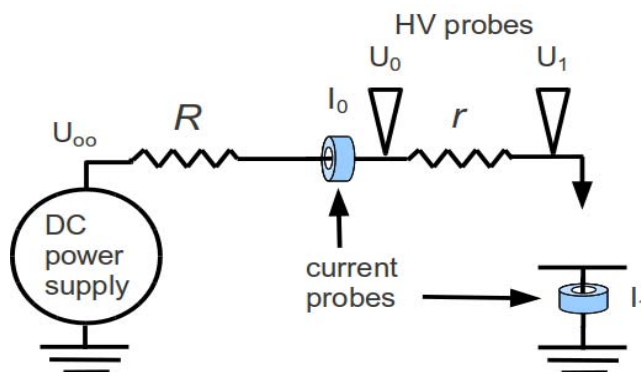
Figure 6. Simplified scheme of experimental setup used to study the influence of external circuit parameters on TS.

3.3.2. Optical diagnostics of TS

Better estimation of electron density in TS requires time-resolved emission spectroscopic study and imaging with fast intensified CCD camera coupled to a monochromator in order to measure the evolution of plasma dimensions and the gas temperature inside the plasma. Optical emission spectroscopy (OES) is a very useful diagnostic technique for identification of active species and radicals in the plasma and for measuring the gas temperature. We therefore also continued investigations of TS by OES techniques.

The optical study of TS is still in progress. We have already obtained several interesting results summarized in the contribution at *International symposium on high pressure low temperature plasma chemistry "HAKONE XII"* (http://neon.dpp.fmph.uniba.sk/hakoneXII//), which is attached in full as Appendix 2.

In summary, TS can be maintained at low energy conditions (0.1-1 mJ/pulse) and the generated plasma cannot therefore reach LTE conditions, although the current pulse can lead to temporary increase of temperature to ~2500 K. The global time-averaged temperature however remains relatively low, since even at repetition frequencies above 10 kHz, each streamer-to-spark process starts at ~450 K.

Subsequent increase of temperature to ~1000 K, accompanied by the increase of the reduced electric field strength inside the plasma channel, governs the streamer-to-spark transition. Shortening of an average streamer-to-spark transition time with increasing TS frequency can be explained by an acceleration of temperature growth.

More research is also needed to explain chemical effects of TS. Emission profiles show that streamer is responsible for significant part of the total emission and for almost all emission of N_2 2nd positive system. This proves the importance of streamer in plasma chemistry, but does not explain why TS was demonstrated more efficient for effects than streamer corona (e.g. in bio-decontamination or flue gas cleaning [7-9]). We suppose that during the initial phase of the spark pulse, the strong chemical effect can be maintained thanks to the combination of a relatively strong reduced electric field (>100 Td) and a high electron density.

Besides interesting results, performed experiments also brought new questions. For example, we observed that streamer to TS transition was governed by the increase of the gas temperature to ~1000 K (Figure 5b in Appendix 2). This increase was faster at higher TS repetition frequencies, leading to faster streamer-to-spark transition (Figure 3b in Appendix 2). The reason for this acceleration will require further research, including kinetic modeling of chemical processes in TS.

3.3.3. Kinetic model of TS

For deeper understanding of TS temporal evolution during the streamer-to-spark phase and the related chemical activity, we started to build a kinetic model of TS. Besides this modeling, we continue with the optical studies, which will be required for the validation of this model. The main part of this work was related to the development of computational package, which can calculate the evolution of species concentration in the plasma, taking into account the pulsed character of TS. The developed package is based on available open source *ZDPlaskin* libraries [12].

Our package is able to characterize both short high current pulse phase of the discharge with fast changes of plasma, and the long relaxation phase (~ms) between the pulses with slow changes of plasma parameters. Time evolution of the reduced electric field strength *E/N* characterizing TS is loaded from an external file. The electron density n_e can be also either loaded from an external file, or calculated by the program itself.

The time evolution of *E/N* and n_e in these external files was estimated from the measured electrical parameters of TS. Detailed description of the procedure for the estimation of n_e can be found in Appendix 1. The profile of *E/N* (*Figure 7*) was in the first approximation derived directly from the measured voltage waveforms, assuming constant value of *E/N* along the TS discharge. Such simplification means that this *E/N* profile is not correct before and during the propagation of the streamer. Even during the later phase, we have to improve the estimate of *E/N* by considering changes of the gas temperature and pressure.

Finally, our developed model was used to calculate the evolution of various species in air plasma generated by TS. Calculated data were qualitatively compared with emission profiles of N_2 (C-B) and O* species experimentally obtained by PMT module (see Figure 4, Appendix 2). Despite the simplification mentioned above, a good agreement was found when both *E/N* and n_e were loaded from external files (*Figure 7*) and we considered the contribution of emission from TS current pulse itself and not from the streamer. On the other hand, significant differences between calculated (*Figure 8*) and experimental emission profiles were observed if n_e was calculated by the model itself. It can be explained by inaccurate approximation of *E/N* profile. We plan to generate sufficiently accurate *E/N* profile, and our model should then presumably generate the same time evolution of n_e as estimated experimentally, which should lead to identical emission profiles as well.
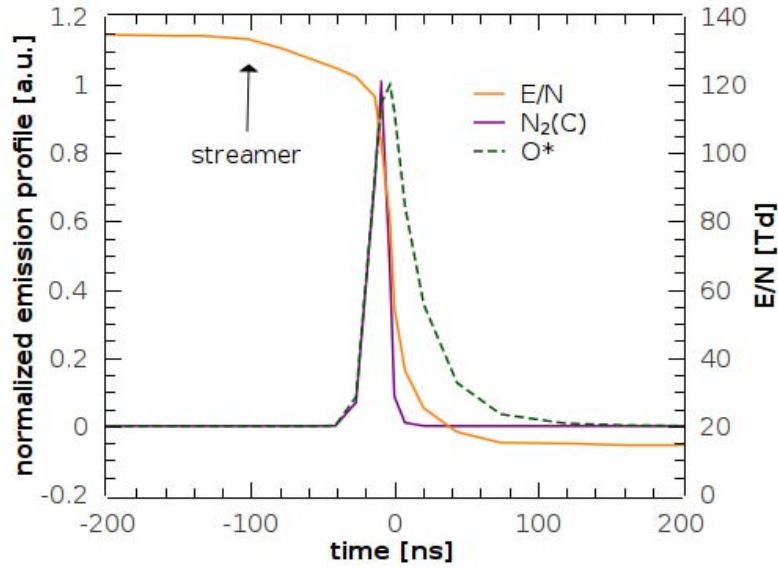

Figure 7. Estimate of E/N and calculated emission profiles of N_2(C) and excited atomic oxygen, obtained using n_e from external file based on experimental data.
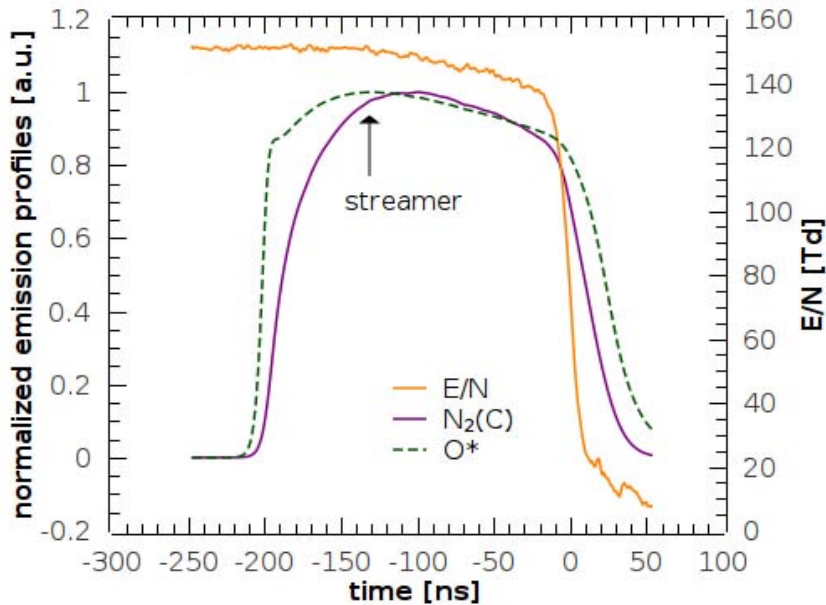

Figure 8. Estimate of E/N and calculated emission profiles of N_2(C) and excited atomic oxygen, obtained during the simulation with n_e calculated internally by kinetic model.

3.3.4. Influence of the gas temperature on TS

In cooperation with the group of our international partner prof. Christophe Laux at Ecole Centrale Paris, Laboratoire EM2C, we recently performed a set of experiments focused on the influence of initial gas temperature T_g on TS. There are several reasons why to be interested in the influence of T_g on TS behavior. First, increased temperature decreases the gas density N, which is generally favorable for plasma scaling. Decreased N also simulates lowered pressure that is of interest for high altitude aircraft shielding. Another example is applying TS for the stabilization of lean flames that normally occur at elevated temperatures. As described in Appendix 2, the streamer-to-spark transition process is governed by the increase of the temperature from an initial value (from 300 to ~450K depending on the TS repetition frequency) to around 1000 K. Thus, experiments with initial temperatures gradually increased up to 1000 K can contribute to the understanding of the processes governing the evolution of TS.

Figure 9 shows the experimental setup used in Paris. Experiments were carried out in atmospheric pressure air preheated with controlled ohmic heater to 300–973 K with an axial flow with velocity from 2 to 10 m/s. The distance between the stainless steel needle electrodes in point-to-plain configuration was 5 mm, anode at the top. A DC High Voltage (HV) power supply HCL 14-20000 connected via a series resistor (R = 10 MΩ) limiting the total current was used to generate a positive TS discharge. The discharge voltage was measured by a high voltage probe LeCroy PMK-14kVAC and the discharge current was measured using a Pearson Electronics 2877 (1V/A) current probe linked to a 350 MHz digitizing oscilloscope LeCroy Waverunner 434 (maximum 2GS/s).

The UV-VIS spectra were obtained using a monochromator (Acton SpectraPro 2500i) fitted with an intensified CCD camera (Princeton Instruments PI-MAX). For time-resolved optical emission measurements, a photomultiplier tube (PMT) module with a 1.4-ns rise time (Hamamatsu H9305-3) was used in place of the monochromator. Its signal was recorded using the oscilloscope. Besides THE total emission, we monitored emission of $N_2(C)$ second positive system by inserting a bandpass interference filter transparent at 337 nm (3nm width) into the optical path.
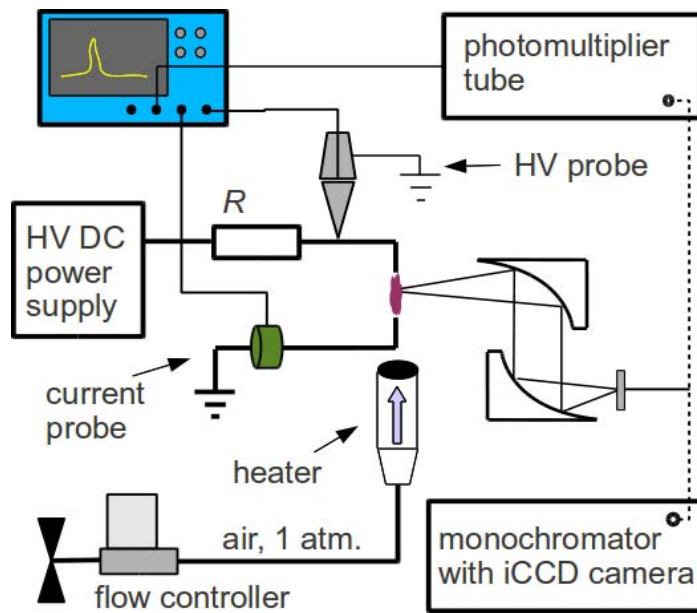

Figure 9. Simplified scheme of experimental setup used to study the influence of gas temperature on TS.

The most obvious influence of an increased T_g on electrical discharges is the decrease of voltage required to initiate them. This is actually caused by the decrease of gas density N. Thus, lower electric field E (and lower applied voltage U_{oo}) is necessary to achieve the same reduced electric field strength E/N necessary to initiate a spark breakdown. We observed this phenomenon for the applied voltage U_{oo} necessary to initiate the TS, approximately determined by solid red line of Figure 10. This figure shows a map of possible discharge regimes which were obtained in our electrical setup at given conditions (flow velocity 2 m/s, gap distance 5 mm, $R = 10$ MΩ) as function of the applied voltage and input T_g. Beside **stable (regular) TS** regime (see also Figure 4b, Appendix 1 for explanation), we observed other discharge regimes:

−   **Unstable TS**: At low U_{oo}, TS has no regular repetition frequency and it may cease and switch to streamer corona; at high U_{oo}, TS may occasionally switch to the glow discharge; at $T_g > 600$ K either to glow or to streamer regime.

−   **Stable streamer**: At low T_g, a typical streamer pulse of some ~10 mA accompanied by no or very small voltage drop. At $T_g > 600$ K, a typical streamer is instantly followed by partial discharging of the capacity C of the electrical setup resulting in stronger (~100 mA) and much longer (~µs) current pulses accompanied by a substantial voltage drop. However, these current pulses are much smaller and longer (~µs) than typical TS pulses (Figure 11) resulting from the total discharging of C. This "elongated" streamer discharging is followed by recharging of C, similar to TS discharge, repeating with a characteristic frequency of ~1–20 kHz, depending on U_{oo}. At $T_g = 973$ K, these streamers and TS pulses become quite similar.

−   **Unstable streamer** is similar to unstable TS discharge regime: at low U_{oo}, streamer has no regular repetition frequency and may cease; at high U_{oo}, streamer pulses are randomly mixed with TS pulses and may occasionally switch to unstable GD regime.

−   **Unstable glow discharge (GD)** is characterized by periods of relatively constant discharge voltage (~2 kV) and constant current (~mA) typical for the glow discharge, occasionally altered with periods of TS or streamer pulses (see also Figure 4c, Appendix 1 for explanation).
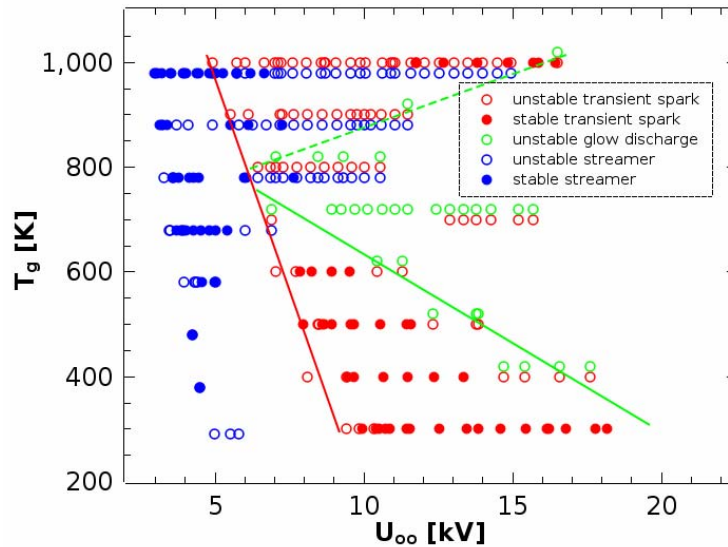

Figure 10. Discharge regimes as function of applied voltage U_{oo} and gas temperature T_g at flow velocity 2 m/s, gap distance 5 mm, R = 10 MΩ. Red solid line – boundary of TS regime, green solid and dashed line - transition to unstable GD regime at lower and higher temperatures, respectively.
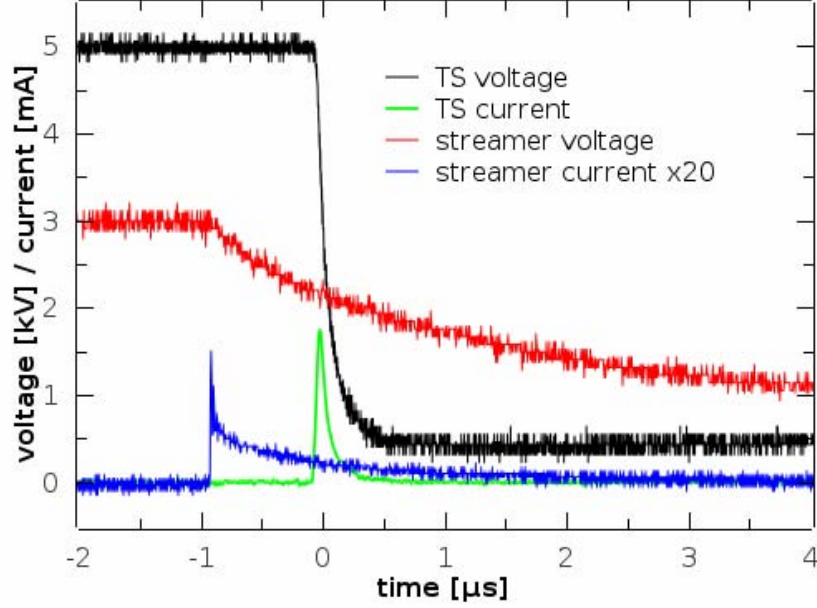
Figure 11. Typical waveforms of streamer regime (current multiplied by 20), T_g = 900 K, U_{oo} = 3.7 kV, compared to ocassional current pulse of unstable TS regime, obtained at T_g = 900 K, U_{oo} = 6.7 kV.

Since we observed the "elongated" streamer for the first time, its understanding will require further research and we do not discuss it in this report. We focus on the changes of TS behavior with increasing T_g.

Thanks to the mechanism of the decrease of gas density N, the increase of T_g also leads to the decrease of TS breakdown voltage U_{TS}. According to equation 4 in Appendix 1, a decrease of U_{TS} implies that lower U_{oo} is necessary to achieve the same TS discharge repetition frequency. This was experimentally confirmed, as shown in Figure 12. Next, we found that the decrease of U_{TS} with growing f observed previously at 300 K (see Fig. 6, Appendix 2), that is caused by an additional gas heating (Appendix 2), happens also at higher temperatures (Figure 13).

We assume that besides the decrease of N, there are other mechanisms related to the increase of T_g, playing role in changes of various discharge regimes. For example, we can see that onset voltage U_{oo} necessary for the transition to unstable GD regime (Figure 10, green solid line) decreases with growing T_g faster than U_{oo} necessary for the appearance of TS regime (Figure 10, red solid line). As a result, at around 700 K, streamer jumps directly to unstable GD and it is not possible to achieve stable TS discharge. Further research is required to identify this mechanism, but we already assume that involved processes depend on the growing T_g so that GD can be established even at lower current than at ambient T_g. Therefore at higher T_g, transition to unstable GD occurs at lower TS mean current I_{mean}, and thus also at lower TS repetition frequency (Figure 14).

It is interesting that further increase of T_g above 800 K leads to the increase of onset voltage U_{oo} necessary for the transition to unstable GD regime (Figure 10, green dashed line). This implies that there is yet another process involved in the mechanism of TS and GD development, which most probably dominates at high temperatures. As a result, stable TS discharge can appear again at ~1000 K. It is also worth mentioning that measurements of time evolution of T_g during the streamer-to-spark process (see Appendix 2) also showed that transition to TS happens when gas temperature increases to about 1000 K. For this reason we suppose that it could be the same process that is responsible for the appearance of stable TS at input T_g = 1000 K.

16

Changes of other TS parameters, such as maximum current I_{max}, duration of the pulses, or energy delivered to gap per pulse (E_p) are not directly dependent of T_g. They can be expressed as functions of U_{TS}, so the dependence on T_g is only indirect via the decrease of U_{TS} with T_g. As a result, we observe the same behavior at all temperatures, such as a decrease of I_{max} and an increase of pulse duration (characterized by full width at half of the maximum FWHM) as U_{TS} decreases (Figure 15 and 16). Total charge and energy per pulse, Q_p and E_p, could be simply calculated from U_{TS} by following formulas:

$$Q_p = C \times U_{TS} \tag{1}$$

$$E_p = \tfrac{1}{2}\, C \times U_{TS}^2 \tag{2}$$

where C is the total capacity of the experimental setup, which we found to be 26 ± 3 pF.
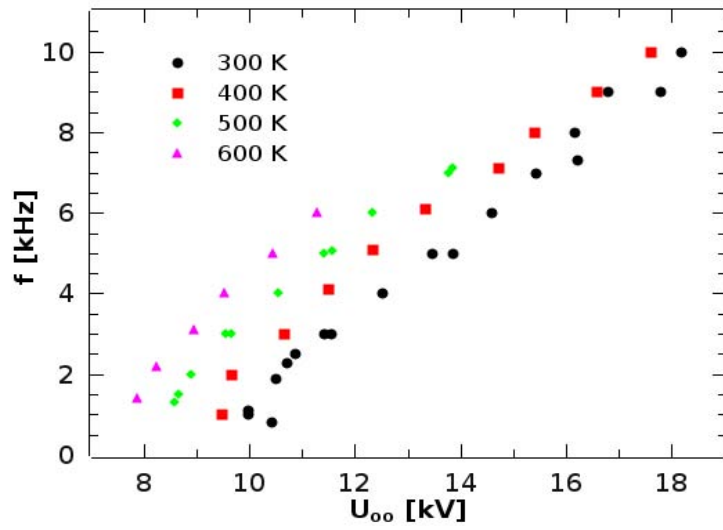
Figure 12. TS repetition frequency f as a function of U_{oo}.
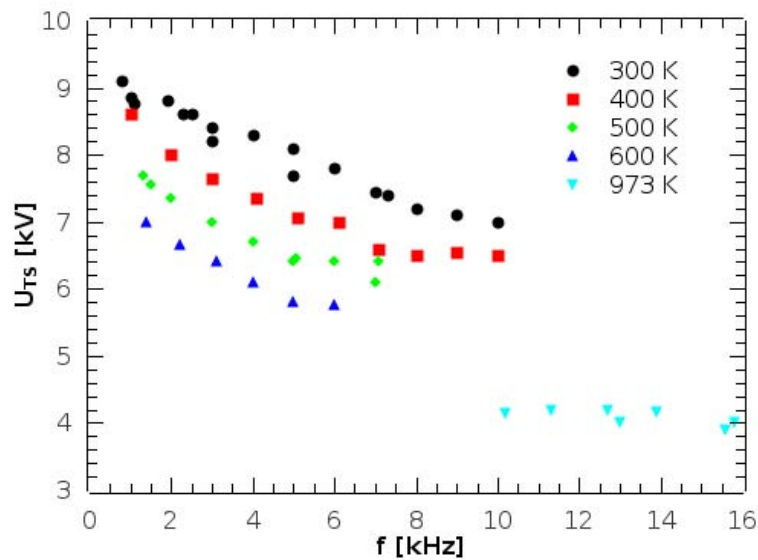
Figure 13. TS breakdown voltage U_{TS} as function of repetition frequency f for various T_g.
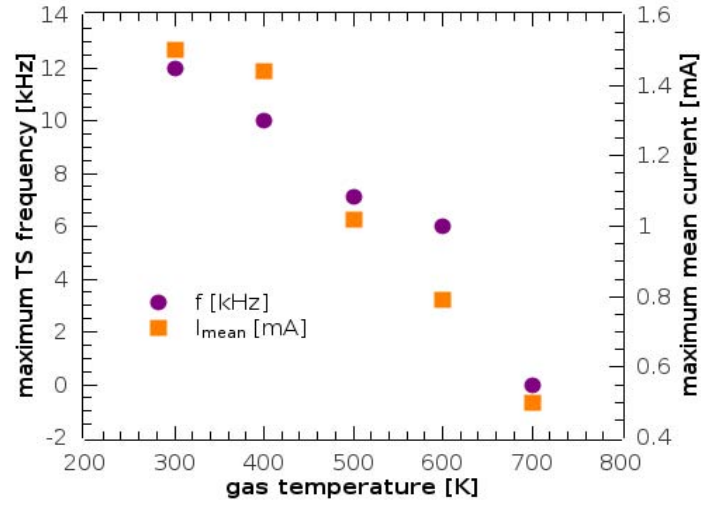
Figure 14. Maximum stable TS repetition frequency f and maximum TS mean current I_{mean} before transition to unstable GD as a function of T_g.
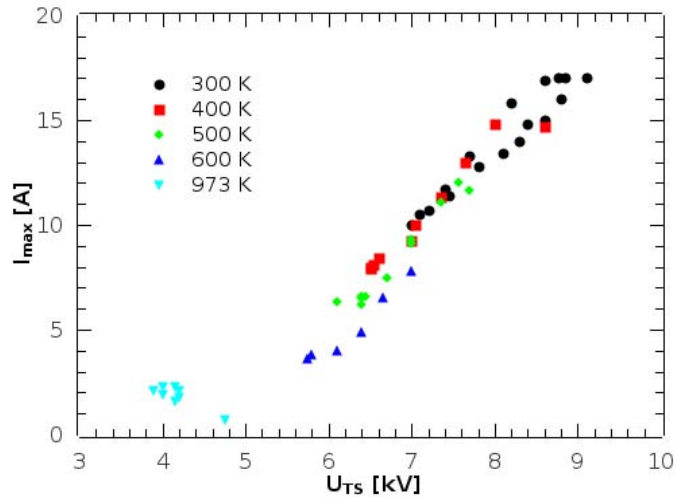
Figure 15. Maximum current of TS pulses as a function of U_{TS} for various T_g.
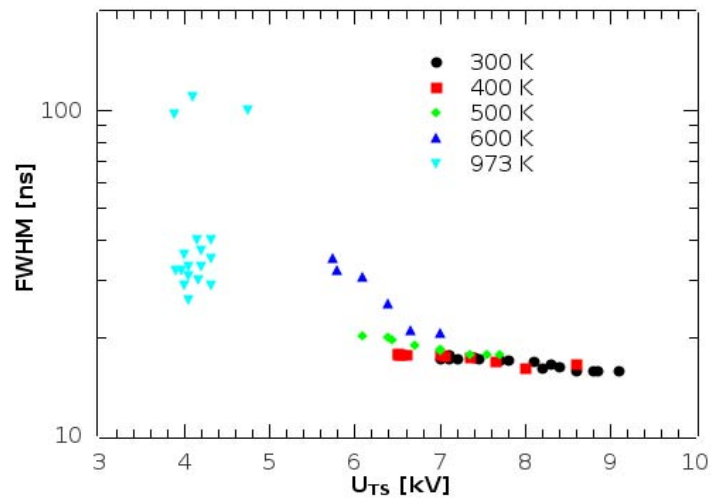
Figure 16. FWHM of TS pulses as a function of U_{TS} for various T_g.

3.3.4. TS in the microwave preheated air

In addition to TS analysis in preheated air to 300-1000 K performed in Paris, we carried out a few experiments with TS in air preheated by our MW plasma torch. The input air T_g was measured by our corona probe method (chapter 3.2) and can be varied by setting the air flow rate and MW power, starting from 1300 K. T_g<1300 K cannot be obtained for the torch ceases. Nevertheless, input T_g above 1300 K is a valuable extension to so far explored 300-1000 K range.

TS was operated between stainless steel pointed needle and another stainless needle electrode positioned horizontally in an axial MW preheated air flow with velocity from 5 to 10 m/s. The anode and the cathode were placed 8 and 3 mm above MW nozzle, respectively, making the TS gap length of 5 mm. Anode needle setup was very similar to that shown in Figure 2. A DC High Voltage (HV) power supply connected via a series resistor ($R = 11$ MΩ) limiting the total current was used to generate a positive TS discharge.

Electrical parameters and time-integrated optical emission spectra of TS were measured in these primary experiments, for 3 pulse frequencies (0.5, 1, and 1.5 kHz). Such spectra provide evaluation of the global (average) gas temperature in the TS channel. The measured temperature profiles along the discharge axis are shown in Figure 17, together with the axial (vertical) profiles of input air temperature measured by the corona probe. TS ads 100-300 K on top of the input gas temperature.

No remarkable discharge regime transitions and discharge stability issues were observed in this input T_g range, although we only worked up to f=1.5 kHz due to limited onset voltage from the power supply. The established TS regime was stable. Detailed temporally-resolved OES of TS in preheated air is planned in near future.

Figure 17. Measured TS temperature axial profiles together with the profiles of input air T_g.

4. Conclusions and perspectives

This annual report summarizes the progress of the current program to investigate the volume scalability and power reduction of nonequilibrium plasmas produced by electrical discharges in atmospheric pressure air, as well as to investigate related fundamental phenomena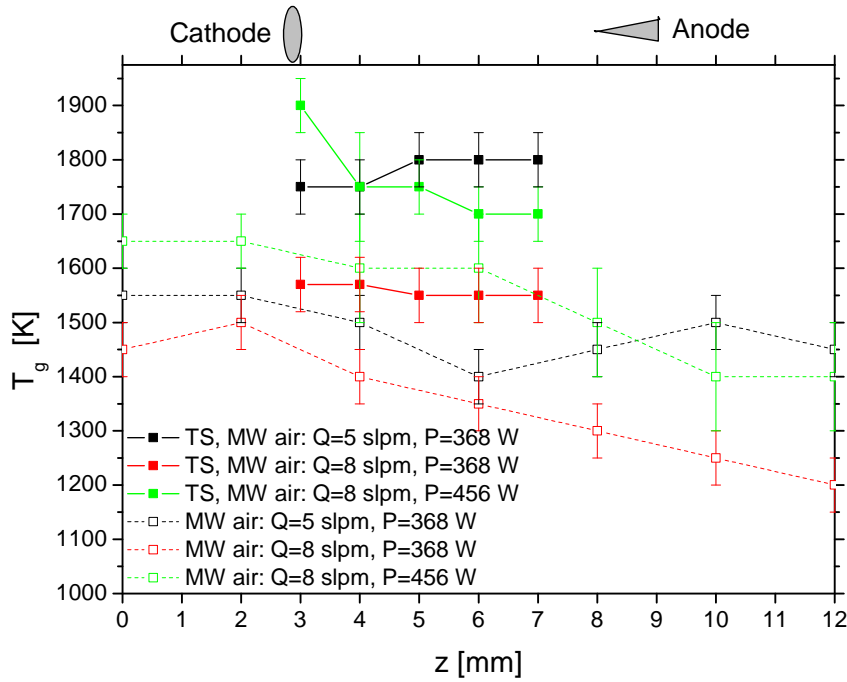. Key results to date demonstrate that both DC glow discharge and pulsed transient spark generate air plasmas of required parameters.

The experiments with DC glow discharge in ambient and preheated air provide basic characteristics of these nonequilibrium atmospheric pressure air plasmas. We developed a novel diagnostics for temperature measurement in the microwave preheated air by using the corona probe and verified its applicability. A journal publication on this novel method is in the review process.

A new concept of the DC-driven pulsed discharge was tested: transient spark, a repetitive streamer-to-spark transition discharge regime of very short pulse duration (~10-100 ns) and with a very limited energy so that the generated plasma is highly nonequilibrium. This discharge can be maintained at low energy conditions by an appropriate choice of the resistances and capacities in the electrical circuit, and its frequency can be controlled by the applied voltage. Here, we specifically investigated the influence of a small separating resistor on the shape and amplitude of the current pulses. Our calculations of temporal evolution of electron density in TS based on detailed analysis of the electrical circuit show that $\sim 10^{16}$ cm^{-3} at maximum and $\sim 10^{11}$ cm^{-3} in average are reached. By setting the parameters of the electric circuit (resistances, capacity) it is possible to control the TS parameters and properties. Another journal publications with these new results is being reviewed and more will be prepared.

We also presented the first results obtained from PMT and ICCD measurements of temporal evolution on nanosecond time scales of highly spectrally-resolved TS emission. The problem of ICCD triggering by the discharge pulse without losing the first 20 ns of the pulse was resolved. Investigating the processes occurring during TS pulse evolution on nanosecond time scales is crucial for deeper understanding of its chemical and physical activity. To this end, we started to build a kinetic model of TS temporal evolution during the streamer-to-spark phase and the related chemical activity.

Transient spark was also studied in preheated air flows. Preheated air decreases the gas density and simulates lowered pressure, which is generally favorable for plasma scaling-up and high altitude aircraft shielding. Applying TS in preheated air is also interesting for the tests of lean flame stabilization. New interesting phenomena and transitions between streamer-spark-glow discharge regimes were revealed as function of input gas temperature.

In the next period we plan further investigations of the temporal evolution of species and processes occurring in TS both in ambient and preheated air flows via ICCD highly temporally and spectrally resolved optical emission spectroscopy combined with electrical measurements and emission via PMT measurements. A comprehensive analysis of the obtained results, as indicated by the preliminary tests, will expectantly lead to for deeper understanding of the elementary processes occurring in these repetitive pulses. The optimum TS conditions with n_e kept above $\sim 10^{12}$ cm^{-3} at all times are sought. Transitions between streamer-spark-glow regimes will be addressed.

We also plan further experiments with glow discharge, also in ambient as well as preheated air. We also envisage testing the GD properties at reduced pressures and comparing the effect of reduced pressure with the elevated temperature.

In cooperation with our French partner we envisage experiments comparing the physical parameters and chemical effects of our DC-driven pulsed TS and their nanosecond repetitively pulsed discharges, both in ambient and preheated air flows. Their respective chemical effects and power budgets will be compared on plasma assisted combustion (lean flame stabilization) and bio-decontamination applications.

In summary, atmospheric pressure air plasmas generated by the glow discharge and transient spark represent a potential for aircraft shielding, plasma assisted combustion, bio-decontamination and other applications. They are worth being further studied.

5. Personnel

Comenius University, Faculty of Mathematics, Physics and Informatics:
Principal investigator: Prof. Zdenko Machala, PhD.
Vice-principal investigator: Mário Janda, PhD.
Other personnel:
Prof. Karol Hensel, PhD.
Prof. Viktor Martišovitš, DSc.
Igor Jedlovský, MSc., Lenka Leštinská, MSc. (PhD students)

International collaboration:
Prof. Christophe O. Laux, PhD., Ecole Centrale Paris, France (consultant)
Dr. Emmanuel Marode, research director at CNRS, Univ. Paris XI, France (consultant)

6. Publications

(since start of preceding EAORD grant in October 2008)

Reviewed papers:

1. L. Leštinská, V. Martišovitš, M. Zahoran, Z. Machala: A*tmospheric pressure microwave plasma for waste carbon treatment*, Chem. Listy **102** (2008) s1428-1431

2. Z. Machala, I. Jedlovský, L. Chládeková, B. Pongrác, D. Giertl, L. Šikurová: *DC discharges in atmospheric air for bio-decontamination – spectroscopic methods for mechanism identification,* Eur. J. Phys. D **47** (2009) 195-204

3. M. Janda, V. Martišovitš, Z. Machala: *Transient spark - DC driven repetitively pulsed discharge and its control by electric circuit parameters,* Plasma Sources Sci. Technol. (2010) submitted

4. L. Leštinská, V. Martišovitš, Z. Machala: *Corona discharge as a diagnostic probe for temperature measurements of atmospheric air microwave plasma,* Plasma Sources Sci. Technol. (2010) submitted

Conference contributions:

Invited:

1. Z. Machala, Bio-decontamination by DC discharges at atmospheric pressure: identification of microbial inactivation mechanisms, invited topical lecture, 29th Int. Conf. Phenomena Ionized Gases, 12-19 July 2009, Cancun, Mexico

Regular:

2. L. Leštinská, Z. Machala: *Corona discharge as a diagnostic probe for temperature measurements of atmospheric microwave plasma*, 19th Int. Symp. Plasma Chemistry, 26-31 July 2009, Bochum, Germany

3. M. Janda, A. Niklová, V. Martišovitš, Z. Machala: *Transient spark - DC driven repetitively pulsed discharge in atmospheric air,* 12th Int. Symp. High Pres. Low Temp. Plasma Chemistry HAKONE XII, Trenčianske Teplice, Slovakia, 12-17 September 2010

4. L. Leštinská, V. Martišovitš, Z. Machala: *Corona discharge as a temperature probe for atmospheric air microwave plasma,* 12th Int. Symp. High Pres. Low Temp. Plasma Chemistry HAKONE XII, Trenčianske Teplice, Slovakia, 12-17 September 2010

7. Honors / Awards

2008 Zdenko Machala, Award of the Slovak Physical Society, 1st-2nd ranking in the Scientific competition of the young researchers

2008 Zdenko Machala, Honorable Award of the Journalist-Studio Bratislava within the awards *"Scientist of the Slovak Republic of the year 2008"*

2009 Zdenko Machala, Slovak vice-prime minister and minister of education prize: *"The personality of science and technology under 35 years"*

8. References

[1] *Mechanisms of Ionizational Nonequilibrium in Air Plasmas,* Final Technical MURI Report, submitted to AFOSR by C.H. Kruger, October 2002

[2] *Scaled-up Nonequilibrium Air Plasmas,* Final Technical Report, submitted to AFOSR by C.H. Kruger, C.O. Laux, Z. Machala, and G.V. Candler, January 2004

[3] *Scaled-up Nonequilibrium Air Plasmas,* Comprehensive Final Report, submitted to EOARD AFOSR by Z. Machala, October 2009

[4] U. Fantz: Plasma Sources Sci. Technol. **15** (2006) S137–S147

[5] Z. Machala, M. Janda, K. Hensel, I. Jedlovský, L. Leštinská, V. Foltin, V. Martišovitš, M. Morvová: J. Mol. Spectrosc. **243** (2007) 194-201

[6] C. O. Laux, T.G. Spence, C.H. Kruger, R.N. Zare: Plasma Sources Sci. Technol. **12** (2003) 125-138

[7] Z. Machala: *Continuous and transient electrical discharges, streamer triggered, at atmospheric pressure, for the removal of Volatile Organic Compounds (VOC)*, PhD. thesis, University Paris-Sud XI, France, Comenius University Bratislava, Slovakia, 2000

[8] Z. Machala, M. Morvová, E. Marode, I. Morva: J. Phys. D: Appl. Phys. **33** (2000) 3198-3213

[9] Z. Machala, I. Jedlovský, L. Chládeková, B. Pongrác, D. Giertl, L. Šikurová: *DC discharges in atmospheric air for bio-decontamination – spectroscopic methods for mechanism identification,* Eur. J. Phys. D **47** (2009) 195-204

[10] D. Z. Pai, G. D. Stancu, D. A. Lacoste, and C. O. Laux: *Nanosecond repetitively pulsed discharges in air at atmospheric pressure—the glow regime,* Plasma Sources Sci. Technol. **18** (2009) 045030

[11] D. Z. Pai, D. A. Lacoste, and C. O. Laux: *Transitions between corona, glow and spark regimes of nanosecond repetitively pulsed discharges in air at atmospheric pressure,* J. Appl. Phys. **107** (2010) 093303

[12] S. Pancheshnyi, B. Eismann, G.J.M. Hagelaar, L.C. Pitchford, *Computer code ZDPlasKin,* http://www.zdplaskin.laplace.univ-tlse.fr, University of Toulouse, LAPLACE, CNRS-UPS-INP, Toulouse, France, 2008.

Appendix 1

Transient spark - DC driven repetitively pulsed discharge and its control by electric circuit parameters

Mario Janda, Viktor Martišovitš and Zdenko Machala

Division of Environmental Physics
Faculty of Mathematics, Physics and Informatics, Comenius University
Mlynska dolina F2, 84248 Bratislava, Slovakia

E-mail: `janda@fmph.uniba.sk`

Abstract. A novel type of streamer-to-spark transition discharge in air at atmospheric pressure is presented. The transient spark (TS) is applicable for flue gas cleaning or bio-decontamination and has a potential in plasma shielding, combustion, and flow control applications. Despite the DC applied voltage, TS has a pulsed character with short ($\sim$10–100 ns) high current ($>$1 A) pulses, with repetitive frequencies 1–20 kHz. Estimation of the temporal evolution of electron density show that $n_e \approx 10^{16}$ cm^{-3} at maximum and $\sim 10^{11}$ cm^{-3} in average are reached using relatively low power delivered to the plasma (0.2–3 W). Thanks to the high repetition frequency, n_e between two current pulses does not fall below a critical value and therefore plasma exists during the whole time. A detailed analysis of the TS control by electrical circuit parameters is presented. With appropriate circuit components, the current pulse tail ($>$1 mA) can be extended and the electron density can be held above $\sim 10^{13}$ cm^{-3} for several tens of μs.

1. Introduction

Atmospheric pressure non-thermal plasmas in air generated by electrical discharges present considerable interest for a wide range of environmental, bio-medical and industrial applications, such as air pollution control, waste water cleaning, bio-decontamination and sterilization, or material and surface treatment [1–6]. In all of these applications, the desired chemical effect is achieved by efficient production of reactive radicals in non-thermal plasma. The key factor for their production are high energy electrons, which can be accelerated by electric field to reach energies of several eV, while the background gas remains cold.

The most simple approach how to generate atmospheric pressure plasma is to apply a DC constant voltage on a couple of metal electrodes. If the generated electric field is

not homogeneous thanks to the geometry of electrodes, e. g. pin-to-plane configuration, a gradual increase of the onset voltage will lead to the generation of corona or streamer corona discharge [7]. Streamers are filamentary structures propagating towards the grounded electrode. Very strong reduced electric field strengths E/N ($\sim$600 Td) and high electron densities n_e ($\sim 10^{14}$ cm^{-3}) can be reached in their head [8]. Streamers can therefore significantly influence the plasma-induced chemistry. However, streamers can also lead to the transition to spark or arc discharge [7,9], generating thermal plasma. Much more power is required to sustain these discharges and the high energy cost allow their utilization only for applications, where one can either expect valuable products (e. g. H_2) or needs to completely destroy very dangerous pollutants [10–12].

One of the most common ways of increasing the breakdown E/N and disabling streamer to spark transition is based on using short high voltage (HV) pulses. It was found that efficiency of active species formation depends on the maximum applied voltage (10–20 kV/cm), voltage rise time (up to 10 ns), decay time ($<$1–10 μs) and total duration of the HV pulse ($<$0.1 μs) [13–16]. The increasing repetition frequency of the HV pulses up to 200 Hz also showed an improved efficiency of removal of various pollutants [16].

HV pulsed devices working at repetition frequencies above 1 kHz appeared only recently [17–20]. The importance of the high repetition frequency on power efficiency of the plasma generation was emphasized [18–20]. The 'glow' regime of nanosecond repetitive pulse (NRP) discharge operating at frequency 30 kHz in air preheated to 1000 K was shown to generate plasma with estimated peak electron density $\approx 10^{13}$ cm^{-3}, while consuming only 1–10 μJ per pulse [20]. A 'spark' regime of NRP, which was already successfully used for stabilization of lean flames [21], was shown to generate plasma with peak electron density $\approx 10^{15}$ cm^{-3}, while consuming only 0.2–1 mJ per pulse [20]. The only disadvantage of this method could be the price of the HV pulse generator.

A restriction of thermal plasma generation when using a cheap DC power supply, can be simply achieved by adding a ballast resistor ($R >$1 MΩ) between the high voltage (HV) electrode and the DC power supply. Since R will limit the average discharge current to several mA, streamer corona will be transformed to either high pressure glow discharge (GD) or transient spark (TS), depending on the gas composition, flow rate, value of R and geometry of electrodes [22–24]. Glow discharge has already been applied e. g. for flue gas cleaning [22,25] and it has a great potential for other applications, such as plasma shielding, since it is a source of stable scalable plasma where $n_e \approx 10^{12}$ cm^{-3} can be achieved. TS discharge regime was first mentioned in [22] and further described in [24]. It has also been successfully applied for several environmental and bio-medical applications [5,22,26].

Transient spark is a relatively new type of discharge, yet its concept is similar to the prevented spark studied in the group of Marode [27–29]. Periods with TS were also observed by Akishev et al. [30], while studying instabilities of GD due to a fast gas flow. TS is a filamentary streamer-to-spark transition discharge initiated by a streamer, which transforms to a short spark pulse due to the discharging of the internal capacity

C of the reactor. TS is based on charging and discharging of C. For typical R and C ($\sim$10 pF), a repetition frequency of this process 1–20 kHz can be achieved. TS represents a simple solution to generate short ($\sim$10–100 ns) high current pulses ($\sim$1–10 A) with high repetition frequency ($\sim$kHz). Our previous time-integrated emission spectroscopy study proved that TS pulses generate highly reactive nonequilibrium plasma with excited atomic radicals (O*, N*), excited molecules N_2^* and ions N_2^{+*}, and gas temperature T_g ranging from 500 to 1500 K, while vibrational temperature T_v was from about 3800 K to 5000 K [5]. In the short pulses of TS, the vibrational-translational energy transfer (VT transfer) does not have sufficient time to develop during the discharge pulse. It can only affect the relaxation phase between the pulses. But there, its effect on gas heating is weak because its time scales are on the contrary much shorter that the typical duration of the relaxation period. Therefore T_g remains fairly low in TS, despite the electrons have high energies. This is a key phenomenon that makes TS discharge very interesting for its low power budget: the discharged energy in one TS pulse is small ($\sim$0.1–1 mJ) and the total power, depending on pulse frequency, is 0.1–2 W. [5, 22].

Various applications have different demands on TS with respect to the optimal frequency, energy per pulse, etc. So the optimization of TS for various applications and better ability to control it by changing electric circuit parameters requires further research.

2. Experimental setup

Figure 1 shows a simplified scheme of the experimental set-up. Experiments were carried out at room temperature in atmospheric pressure air with a gas flow perpendicular to discharge channel with a velocity $\sim$20 cm.s^{-1}. A stainless steel needle was used as a high voltage (HV) electrode opposite to a grounded planar copper electrode. The distance between electrodes d=5 mm. A DC High Voltage (HV) power supply connected via a series resistor R limiting the total current was used to generate a positive TS discharge. The value of R varied from 3.5 to 9.84 MΩ. Additional small resistor r, the effect of which we further studied, was attached directly to the HV electrode, separating it thus from a HV cable connecting it with the resistor R (Fig. 1). The value of r varied from 0 (no r) to 110 kΩ.

The discharge voltage was measured by two 100 MΩ high voltage probes (Tektronix P6015A) at both ends of the resistor r. The reason why we stressed here the presence and the position of is its influence on TS properties. The length of the HV cable between the resistor R and the HV electrode can significantly contribute to the total capacity C discharging during each TS pulse. We tested different cables with lengths from 0.3 to 2 m, having capacities from approximately 5 to 34 pF. The currents at the grounded electrode and between R and r were measured by a Pearson Electronics 2877 (1V/A) and a Pearson Electronics 4100 (1V/A) current probes. All current and HV probes were linked to the 200 MHz digitising oscilloscope Tektronix TDS2024.

3. Results and Discussion

3.1. Introduction to Transient Spark

When the high voltage U_{00} applied to the stressed electrode is progressively increased, we first observe a streamer corona. When the breakdown voltage is reached, a transition to transient spark occurs at the discharge voltage U_{TS}. TS is a filamentary streamer-to-spark transition discharge initiated by a streamer (phase A, Fig. 3a), which transforms to a short spark pulse (phase B, Fig. 3a). Figure 2 shows typical look of TS.

The TS current pulse is due to the discharging of the capacity C, composed of several components (internal capacity of the discharge chamber C_{int}, capacity of the high voltage cable C_{cable} between the ballast resistor R and the electrode, and capacity of the HV probe $C_{HV} = 3\,\mathrm{pF}$). When C is discharged, the current approximately given by

$$I_1(t) \approx -C\,\frac{\mathrm{d}U_1(t)}{\mathrm{d}t} \tag{1}$$

reaches a high value ($\sim 1\,\mathrm{A}$) and the voltage drops to almost zero (phase C, Fig. 3a). Then, during the quenched phase (phase D, Fig. 3b), C is recharged by a growing potential U_1 on the stressed electrode. The growth of the potential U_1 in time t can be in the first approximation described by the following equation:

$$U_1(t) = U_{oo}\left[1 - \exp\left(\frac{-t}{RC}\right)\right]. \tag{2}$$

Usually, during this relaxation phase when the gap potential reaches a specific threshold, corona discharge appears, and some pre-breakdown streamers (phase E, Fig. 3a,b). A new TS pulse occurs in time $t = T$, at breakdown voltage U_{TS} given according to (2) by:

$$U_{TS} = U_{oo}\left[1 - \exp\left(\frac{-T}{RC}\right)\right]. \tag{3}$$

From (3) we get the characteristic repetition frequency f of this process:

$$f = \frac{1}{T} = \frac{1}{RC\ln\left[\frac{U_{oo}}{(U_{oo}-U_{TS})}\right]}. \tag{4}$$

However, the repetition frequency f of the first TS pulses, when U_{00} only slightly exceeds U_{TS} is low and very irregular (Fig. 4a). Further increase of U_{00} leads to an increase of f and TS pulses become more regular (Fig. 4b). For typical R and C, the repetition frequency f is in the order of several kHz and grows with increasing U_{00} (Fig. 5). However, even with known values of C and R, formula (4) is not reliable to predict the growth of f with U_{00}, because U_{TS} also depends on f (Fig. 6). The decrease of U_{TS} with f can be explained by the increasing gas temperature T_g, resulting in a decreasing gas density N. Since some threshold, the reduced electric field E/N is sufficient to initiate the TS pulse, E and thus also U_{TS} may be now lowered [31]. Another reason may be memory effects – the gap remains pre-ionized by previous TS pulses as f increases.

3.2. Transient spark control by electric circuit parameters

The RC term determines which frequencies can be achieved and how fast f grows with U_{00} (Fig. 5), but R and C also influence other TS properties. The major role of R is to avoid the transition to arc or the glow discharge (GD), because the increase of f is accompanied by the increase of mean current I_{mean} (Fig. 7). As I_{mean} exceeds approximately $1.5\,\mathrm{mA}$, TS tends to transform into a pulse-less GD regime with a constant current of few mA (phase F, Fig. 3b). However, due to the high value of R and the electro-negativity of air, this regime is not stable and the discharge randomly switches between the glow regime and the high frequency TS regime (Fig. 4c). Typically, R should be above 5 MΩ to avoid transition to a stable glow discharge. On the other hand, if $R > 10\,\mathrm{M\Omega}$, the energy losses on the external resistor become too high for operating at high f. So the TS properties cannot be controlled by changing the value of R only.

The influence of C on TS is even more significant. Since TS is based on charging and discharging of C, a total charge Q_p, and the energy delivered to the discharge gap per pulse E_p are functions of C. We can therefore affect the shape of TS current pulses by changing C. Larger C typically means larger current pulses. However, we must also take into account the dependence of the current pulse maximum I_{max} and current pulse width (FWHM) on f. With increasing f, pulses get smaller and broader (Fig. 6). The increase of I_{max} with increasing C is therefore observed only at constant f.

However, the question is how to control C? It consists of several components, from which one can easily change only the value of C_{cable} by changing the cable length. Longer cable means larger C_{cable}. However, it is not very practical to change C by using different HV cables with various lengths. So we use long cables ($C_{cable} > 20\,\mathrm{pF}$) and to place a small separating resistor r between the HV electrode and HV cable. This r separates C_{cable} from $C_{int} + C_{HV}$. Like this, we were able to control the shape of the current pulse by changing r, without changing C_{cable}.

3.3. The influence of separating resistance r on TS

We expected that the increasing value of r would lead to gradual decrease of I_{max}. This tendency was experimentally confirmed (Fig. 8), but the dependence of the pulse shape and width on r was not the expected monotonous increase. We found that FWHM is not a proper parameter to describe TS pulses, since they are obviously formed by a convolution of two independend current pulses (Fig. 9). The first one (I_{C1}) is due to discharging of the capacity $C'_1 = C_{int} + C_{HV}$ in the gap. The second one (I_0) is due to discharging of the HV cable through the resistor r.

These two currents, I_{C1} and I_0, can explain the dependences of I_{max} and pulse shape on r. While I_{C1} does not change significantly with r (Fig. 8, 1st peak), I_0 gets smaller (Fig. 8, 2nd peak) and broader. As a result, I_{max} also decreases with r, but when the maximum of I_0 becames small compared to the maximum of I_{C1}, I_{max} remains almost constant for a further increase of r (Fig. 8, $r > 10\,\mathrm{k\Omega}$). Here we obtained I_0 from I_1

after subtraction of I_{C1}. C_1' necessary to calculate I_{C1} was obtained by fitting measured current waveforms by (5) for large r.

We expected that I_0 can be also derived from the measured potential drop on r:

$$I_1(t) \approx I_{C_1} + I_0 = -C_1' \frac{dU_1(t)}{dt} + \frac{U_0 - U_1}{r}. \tag{5}$$

We experimentally tested the validity of (5) by measuring current I_0 flowing through r (Fig. 10). However, the agreement between the measured current and the current calculated from U_0 and U_1 was good enough only for $r > 1.5\,\text{k}\Omega$. For smaller r, experimental results were in agreement only with I_0 derived from I_1 after subtraction of I_{C1}. In order to find a better formula for $I_1(t)$, which would enable us to calculate it from the measured voltage waveforms for all values of r, we performed a detailed analysis of the electric circuit representing our experimental setup.

3.4. Analysis of the electric circuit representing TS

Figure 11 shows a simplified electric circuit representing TS. Here, the separating resistor is characterized not only by its resistance r, but also by its inductance L_0. We found it to be crucial to explain the observed oscillations of the measured current and voltage waveforms. We even have to include the inductance L_1 of the cable from the planar low voltage electrode to ground. For this reason we also had to divide C_{int} into two parts. The first one, C_{el}, represents the capacity of electrodes. The second one is included in C_1.

The utilization of the HV probes also introduces a resistance $R_{HV} = 100\,\text{M}\Omega$ through which a parasitic loss currents pass. The capacity of these probes is included in C_0 and C_1, respectively. The discharge plasma is represented by its resistance R_p. The plasma resistance is unknown and changes in time. This is the parameter responsible for a pulsed character of TS. If we know R_p, we would be able to describe all parameters of this circuit (U_1, I_1, ...) from the voltage and the current provided by the HV power supply. On the contrary, from the measured values of U_0, U_1 and I_1 we can derive the time variations of R_p. From R_p, we can estimate the plasma conductivity and thus the electron density.

First of all, let us find the dependence of I_1 on U_0 and U_1 starting from the basic equations describing the electric circuit

$$I_1 = I_0 - \frac{U_1}{R_{HV}} - C_1 \frac{dU_1}{dt}, \tag{6}$$

$$U_1 = U_0 - rI_0 - L_0 \frac{dI_0}{dt}. \tag{7}$$

If r is sufficiently high compared to L_0, the third term in (7) can be neglected and from combination of (6) and (7) we get

$$I_1(t) = -C_1 \frac{dU_1(t)}{dt} + \frac{U_0 - U_1}{r} - \frac{U_1}{R_{HV}}. \tag{8}$$

This is actually an equivalent of the equation (5), corrected by the current lost through R_{HV}. If L_0 can be neglected, C_1 becomes equal to C_1', because C_{el} can be now added to C_1. If the inductance term in (7) cannot be neglected, we must use another equation obtained from the analysis of the circuit:

$$I_0 = I_{00} - \frac{U_0}{R_{HV}} - C_0 \frac{\mathrm{d}U_0}{\mathrm{d}t}, \tag{9}$$

where

$$I_{00} = \frac{U_{00} - U_0}{R}. \tag{10}$$

From the combination of (6) and (9) we get

$$I_1 = \frac{U_{00} - U_0}{R} - \frac{U_0 + U_1}{R_{HV}} - C_0 \frac{\mathrm{d}U_0}{\mathrm{d}t} - C_1 \frac{\mathrm{d}U_1}{\mathrm{d}t}. \tag{11}$$

The 1st term is feeding current from the power supply, the second one is a current lost through R_{HV}. During the TS high current pulse (phase B), these two terms are negligible, but they are important to estimate the current during phases C and E. The last two terms of (11) dominate during the phase B and they correspond to two current terms in (5), but they are now both expressed as capacitive currents. Capacity C_0 is the sum of C_{cable} and C_{HV} of the 2nd HV probe. Validity of this formula was again checked by fitting the measured waveforms of I_1 and I_0. For the longest 2 m HV cable we thus obtained values of $C_0 = 37 \pm 3 \,\mathrm{pF}$ and $C_1 = 7 \pm 1 \,\mathrm{pF}$, which could be used to obtain I_1 from U_0 and U_1 for every value of r.

However, the problem of (11) is that it deos not directly describe the dependence of TS parameters on r, which is not even included there. Moreover, we also wanted to find relations between U_0, U_1, and I_1, which would enable us to reduce the number of parameters we have to measure during the experiments. In order to reduce the number of required HV probes, we need to describe U_1 as a function of U_0. We can obtain it after we add derivative of (9) into (7):

$$U_1 = (1 + r\rho)U_0 - \frac{r}{R}U_{00} + (rC_0 + \rho L_0)\frac{\mathrm{d}U_0}{\mathrm{d}t} + L_0 C_0 \frac{\mathrm{d}^2 U_0}{\mathrm{d}t^2}, \tag{12}$$

where

$$\rho = \frac{R + R_{HV}}{R_{HV} R}. \tag{13}$$

Here we could neglect the term with the derivative of U_{00}. Finally, from the combination of (11) and (12) we get the dependence of I_1 on U_0, which also directly includes the influences of r, C_0, C_1 and L_0:

$$I_1 = c_{00} U_{00} + c_0 U_0 + c_1 \frac{\mathrm{d}U_0}{\mathrm{d}t} + c_2 \frac{\mathrm{d}^2 U_0}{\mathrm{d}t^2} + c_3 \frac{\mathrm{d}^3 U_0}{\mathrm{d}t^3} \tag{14}$$

where

$$c_{00} = \frac{r + R_{HV}}{R_{HV} R} \tag{15}$$

$$c_0 = -\frac{rR + rR_{HV} + 2R_{HV}R + R_{HV}^2}{RR_{HV}^2} \tag{16}$$

$$c_1 = -C_0 - (1 + r\rho)C_1 - \frac{rC_0}{R_{HV}} - \frac{\rho L_0}{R_{HV}} \tag{17}$$

$$c_2 = -rC_1C_0 - \rho C_1 L_0 - \frac{L_0 C_0}{R_{HV}} \tag{18}$$

and

$$c_3 = -L_0 C_1 C_0. \tag{19}$$

The validity of (12) and (14) was also tested and confirmed by fittig measured waveforms. However, due to a large error coming from the tripple numerical derivative of the measured U_0, it is more accurate to use equations (11) or (5), depending on r, to calculate I_1 during the current phase of TS. Equation (14) is rather useful to estimate the background and parasite currents (first two terms).

3.5. Estimation of the plasma resistance and electron density

We can use the dependence of the electron number density on the plasma conductivity σ_p to calculate n_e:

$$n_e = \frac{\sigma_p m_e \nu_c}{e^2}. \tag{20}$$

Here e and m_e are the electron charge and mass, respectively, and ν_c is the electron-heavy particles collision frequency. The plasma conductivity σ_p is related to the plasma resistance R_p by

$$\sigma_p = \frac{d}{R_p A}, \tag{21}$$

where d and A are the gap length and the cross-sectional area of the plasma channel, respectively. A formula describing the dependence of R_p on the discharge voltage and current can be obtained by an analysis of the electric circuit representing TS. We get

$$R_p = \frac{U_1 - L_1 \frac{dI_1}{dt}}{I_1 - C_{el}\frac{dU_1}{dt} + L_1 C_{el}\frac{d^2 I_1}{dt^2}}. \tag{22}$$

From this equation, R_p can be calculated if we know values of L_1 and C_{el}. We minimized the influence of L_1 using the shortest possible grounding wires ($\sim$10 cm), with estimated inductance $\sim$100 nH. For this reason, the influence of L_1 is not negligible only for very sharp high current pulses ($I_{max} > 5$ A and pulse width $\sim$10 ns) with large derivative of I_1. These high pulses appear only at frequencies below 2 kHz, if the total capacity of the system $C > 20$ pF and if the separating resistor r is very small ($r < 0.5$ kΩ). For all estimates of R_p presented here can be therefore the influence of L_1 neglected. This mean that the term $C_{el}\frac{dU_1}{dt}$ can be also neglected, because without L_1, C_{el} can be added to C_1 and I_1 is equal to I_p.

Under these simplifications, we can estimate R_p directly from the measured U_1 and I_1, but we also used (14) to better estimate I_1 before and after the high current pulse. Moreover, U_1 is not measured accurately enough by the HV probe at the beginning of the phase B of TS, when it falls to very low values. For this reason, we estimated R_p

also from I_0 and U_0, because U_0 does not drop to very low values for $r > 1.5\,\text{k}\Omega$. When C_1 is already discharged, the following equation can be used:

$$R_p = \frac{U_0}{I_{00} - \frac{U_0}{R_{HV}} - C_0 \frac{\mathrm{d}U_0}{\mathrm{d}t}} - r. \tag{23}$$

Besides the uncertainty of R_p, the plasma diameter D_p, necessary to calculate A, and ν_c are another major sources of uncertainty in the estimation of n_e. We calculated ν_c in air for T_g from 300 to 1500 K and for E/N from 10 to 200 Td using our package for Monte Carlo simulation of electron dynamics [32]. We found that ν_c can vary from approximately 4×10^{11} to 4×10^{12} s^{-1}. We use the constant value 10^{12} s^{-1} to estimate n_e in TS. This approximation introduces the uncertainty of less than a factor 4.

D_p changes in time and it can be well defined only for certain phases of TS discharge (phases A-C). Based on our preliminary experiments with TS imaging by iCCD camera, we estimated the plasma channel diameter to $\sim$200 μm during the spark pulse. This is in a good agreement with a value reported by Naidis [33] from numerical simulation of the streamer-to-spark transition dynamics. Later phase of TS with current around 1 mA is similar to a glow discharge. The diameter of a stable GD channel is around 500 μm [5], and we suppose that this value can be used in the first approximation as the upper limit of TS plasma channel diameter. Since we do not know an exact time evolution of D_p we took a constant value $D_p = 200\,\mu$m. This approximation introduces the uncertainty less than a factor 3 for the phases A-C. It is questionable whether we can approximate the plasma by a column in later phases D and E. Even if yes, its expansion should be included. Values of n_e estimated for these phases are therefore only informative. Altogether, we can estimate n_e not better than with the uncertainty of factor 10. Better approximation will require the time resolved measurements of gas temperature and plasma diameter in TS.

Figure 12 shows a typical time evolution of R_p and n_e for TS with no separating resistor r and a repetition frequency $\sim$2 kHz in two different time scales. Fig. 12a zooms on the high current phase of TS, whereas Fig. 12b shows the estimate of R_p and n_e during several TS cycles. As we can see, the initial n_e, even before bridging of the gap by a streamer, is relatively high. Values from around 10^{10} to 10^{13} cm^{-3} were observed, though this value is only informative, as was mentioned above. This high concentration can be explained by preliminary streamers and corona discharge phase of TS, but also by a memory effect - these electrons can remain from previous pulse thanks to the high f. During the short spark pulse, R_p drops down to few hundred ohms and n_e can reach $\sim$10^{16} cm^{-3}. As soon as C is discharged, n_e drops quickly to about 10^{14} cm^{-3}. After the TS pulse, n_e gradually decreases to about 10^{10}–10^{11} cm^{-3} (Fig. 12b). In reality it should be lower, because we did not include the expansion of plasma channel in this estimation. However, even if the volume of plasma expands by two orders of magnitude (average diameter 2 mm), the lowest n_e would be in the order of 10^8–10^9 cm^{-3}. In this case, the Debye length would be not larger than 0.2 mm (calculated for T_e=1000 K and $n_e = 10^8$ cm^{-3}) which is by one order of magnitude smaller than the assumed plasma dimension. We can therefore suppose that plasma

exists during the whole period of TS, even during the relaxation phase, although its resistance becomes quite high ($R_p \sim 10^8\,\text{M}\Omega$).

Fig. 12b also shows a short period of the unstable GD regime and for this period we obtained $n_e \approx 10^{12}\,\text{cm}^{-3}$. This is in a very good agreement with previous studies of GD [5], where n_e was estimated from the current density. This fact confirms that our calculated values of n_e are reasonable.

3.6. Influence of r on R_p and n_e

Increasing value of r leads to a decrease of I_{max} and therefore also to lower maximum n_e (Fig. 13). On the other hand, increasing r causes that it takes longer for C_0 to be discharged - up to $\sim 20\,\mu s$ for $r = 111\,\text{k}\Omega$ (Fig. 13). This prolongation of the current tail means that n_e stays relatively high longer. Typical n_e at the end of discharging of C_0 was $\sim 10^{13}\,\text{cm}^{-3}$. We also estimated that it takes up to $\sim 100\,\mu s$ ($r = 111\,\text{k}\Omega$) for n_e to drop below $\sim 10^{12}\,\text{cm}^{-3}$. Thus, higher r enables to merge the characteristics of TS and GD together, i. e. relatively high current pulse ($\sim 2\,\text{A}$) with high efficiency of production of radicals are followed by long period with current above $1\,\text{mA}$, during which plasma reaches characteristics typical for GD.

On the other hand, the voltage U_0 does not drop to low values for larger r, e. g. for $r = 27\,\text{k}\Omega$, $U_0^{min} \approx 1.5$ kV, and so C_0 cannot be discharged completely. It is therefore not suitable to use larger values of r. The separating resistor r must remain much smaller than the ballast resistor R, otherwise the discharging of C_0 has negligible effect on the discharge current and $r + R$ can be treated as one resistor.

4. Conclusions

A new concept of a DC-driven pulsed discharge was investigated: transient spark, a repetitive streamer-to-spark transition discharge of very short pulse duration ($\sim$10-100 ns) and with a very limited energy so that the generated plasma is highly non-equilibrium. This discharge can be maintained at low energy conditions (up to $1\,\text{mJ/pulse}$) by an appropriate choice of the resistances and capacities in the electrical circuit, and its frequency can be controlled by the applied voltage. The activity of transient spark is comparable with the nanosecond repetitive pulsed discharges but its advantage is an ease of the DC operation and no need of special and expensive high voltage pulsers with high repetitive frequency and nanosecond rise-times.

Our calculations of temporal evolution of electron density in TS based on the detailed analysis of the electrical circuit showed that $n_e \approx 10^{16}\,\text{cm}^{-3}$ at maximum and $\sim 10^{11}\,\text{cm}^{-3}$ in average are reached. Better estimation of these values will require further time-resolved emission spectroscopic study and imaging with fast iCCD camera coupled to a monochromator in order to estimate the evolution of plasma dimensions and the gas temperature inside the plasma. These investigations are on the way and will be a subject of the following paper.

The influence of a resistor r separating the HV cable from the HV electrode on the TS properties was presented here. The increasing r causes that it takes much longer to discharge the charge stored in the HV cable and the tail of the current pulse can be thus longer than several tens of μs. This additional resistor r enables to merge the characteristics of TS and the glow discharge together, i. e. relatively high current pulses ($\sim$1 A) with a high efficiency of radical production are followed by long periods with the current above 1 mA during which plasma reaches characteristics typical for GD. Our further research in this area will be focused on scaling up the TS discharge to produce larger volumes of non-equilibrium air plasma and to reduce the power budget.

Acknowledgments

References

[1] L. Civitano. *Non-Thermal Plasma Techniques for Pollution Control*, volume 1 of *NATO Series*. Springer, New York, 1993.

[2] A.A. Joshi, B.R. Locke, P. Arce, and W.C. Finney. *Journal of Hazardous Materials*, 41:3, 1995.

[3] M. Laroussi. *IEEE Trans. Plasma Sci.*, 30:1409, 2002.

[4] J. Pawlat, K. Hensel, and S. Ihara. *Acta Phys. Slovaca*, 55:479, 2005.

[5] Z. Machala, M. Janda, K. Hensel, I. Jedlovsky, L. Lestinska, V. Foltin, V. Martisovits, and M. Morvová. *J. Mol. Spectrosc.*, 243:194, 2007.

[6] M. Cernak, J. Rahel, D. Kovacik, M. Simor, A. Brablec, and P. Slavicek. *Contrib. Plasma Phys.*, 44:492, 2004.

[7] L.B. Loeb. *Electrical Coronas*. University of California Press, Berkeley, 1965.

[8] A.A. Kulikovsky. *IEEE Trans. Plasma Sci.*, 25:439, 1997.

[9] H. Raether. *Electron Avalanches and Breakdown in Gases*. Butterworths, London, 1964.

[10] A. Kobayashi, K. Osaki, and C. Yamabe. Treatment of CO2 gas by high-energy type plasma. *Vacuum*, 65(3-4):475–479, 2002.

[11] L. Bromberg, D.R. Cohn, A. Rabinovich, and N. Alexeev. Plasma catalytic reforming of methane. *Int. J. of Hydrogen Energy*, 24(12):1131–1137, 1999.

[12] A. Kanzawa. Chemical reaction in a thermal plasma. *Plasma Sources Sci. Technol.*, 2(1), 1993.

[13] A. Mizuno, J.S. Clements, and R.H. Davis. A method for the removal of sulfur-dioxide from exhaust-gas utilizing pulsed streamer corona for electron energization. *IEEE Trans. on Indus. Applic.*, 22(3):516–522, 1986.

[14] J.J. Lowke and R. Morrow. Theoretical analysis of removal of oxides of sulfur and nitrogen in pulsed operation of electrostatic precipitators. *IEEE Trans. on Plasma Sci.*, 23(4):661–671, 1995.

[15] B.M. Penetrante, J.N. Bardsley, and M.C. Hsiao. Kinetic analysis of non-thermal plasmas used for pollution control. *Jpn. J. Appl. Phys.*, 36(7B):5007–5017, 1997.

[16] S. Masuda and H. Nakao. Control of NOx by positive and negative pulsed corona discharges. *IEEE Trans. on Indus. Applic.*, 26(2):374–383, 1990.

[17] J.L. Walsh, J.J. Shi, and M.G. Kong. Submicrosecond pulsed atmospheric glow discharges sustained without dielectric barriers at kilohertz frequencies. *Appl. Phys. Lett.*, 89(16), 2006.

[18] S.V. Pancheshnyi, D.A. Lacoste, A. Bourdon, and C.O. Laux. Ignition of propane-air mixtures by a repetitively pulsed nanosecond discharge. *IEEE Trans. Plasma Sci.*, 34(6, Part 1):2478–2487, 2006.

[19] D. Pai, D.A. Lacoste, and C.O. Laux. Images of nanosecond repetitively pulsed plasmas in preheated air at atmospheric pressure. *IEEE Trans. Plasma Sci.*, 36(4, Part 1):974–975, 2008.

[20] D. Pai, G.D. Stancu, D.A. Lacoste, and C.O. Laux. *Plasma Sources Sci. Technol.*, 18:045030, 2009.

[21] G. Pilla, D. Galley, D.A. Lacoste, F. Lacas, D. Veynante, and C.O. Laux. *IEEE Trans. Plasma Sci.*, 34:2471, 2006.

[22] Z. Machala, M. Morvova, E. Marode, and I. Morva. *J. Phys. D: Appl. Phys.*, 33:3198, 2000.

[23] Y Akishev, O Goossens, T Callebaut, C Leys, A Napartovich, and N Trushkin. The influence of electrode geometry and gas flow on corona-to-glow and glow-to-spark threshold currents in air. *J. Phys. D: Appl. Phys.*, 34(18):2875–2882, 2001.

[24] Z. Machala, I. Jedlovsky, and V. Martisovits. DC discharges in atmospheric air and their transitions. *IEEE Trans. on Plasma Sci.*, 36(4, Part 1):918–919, 2008.

[25] Y.S. Akishev, A.A. Deryugin, I.V. Kochetov, A.P. Napartovich, and N.I. Trushkin. DC glow-discharge in air-flow at atmospheric-pressure in connection with waste gases treatment. *J. Phys. D: Appl. Phys.*, 26(10):1630–1637, 1993.

[26] Z. Machala et al. *Eur. Phys. J. D*, 54:195, 2009.

[27] F. Bastien and E. Marode. *J. Phys. D: Appl. Phys.*, 12:249, 1979.

[28] E. Marode, A. Goldman, and M. Goldman. *Non-Thermal plasma techniques for pollution control*, chapter High pressure discharge as a trigger for pollution control, pages 167–190. NATO ASI series, Part A. Springler-Verlag, Berlin Heidelberg, 1993.

[29] R. Hafez, S. Samson, and E. Marode. A prevented spark reactor for pollutant control. investigatin of no$_x$ removal. In 12th *ISPC*, pages 855–861, 1995.

[30] Yu. Akishev, M. Grushin, V. Karalnik, A. Petryakov, and N. Trushkin. *J. Phys. D: Appl. Phys.*, 43:075202, 2010.

[31] M. Janda and Z. Machala. Transient spark discharge in N2/CO2/H2O mixtures at atmospheric pressure. *IEEE Trans. Plasma Sci.*, 36(4):916, 2008.

[32] M. Janda et al. *Eur. Phys. J. D*, 45:309, 2007.

[33] G.V. Naidis. Simulation of streamer-induced pulsed discharges in atmospheric-pressure air. *Eur. Phys. J. Appl. Phys.*, 47:22803, 2009.
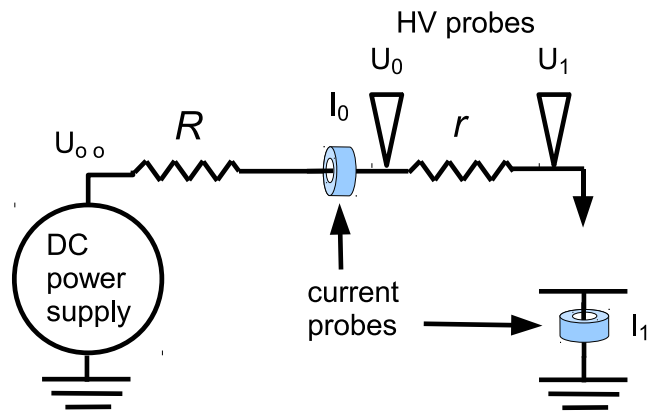
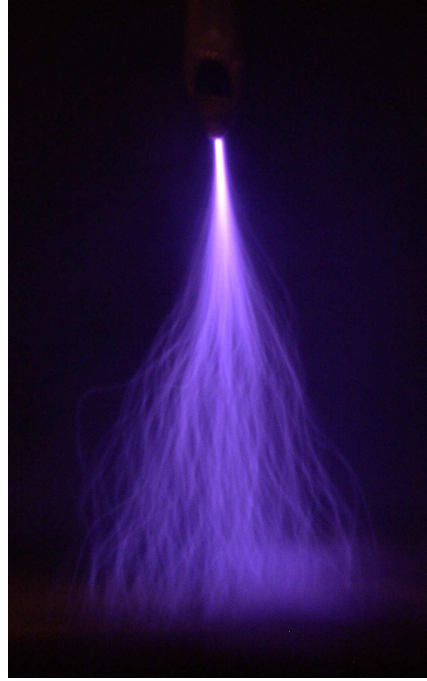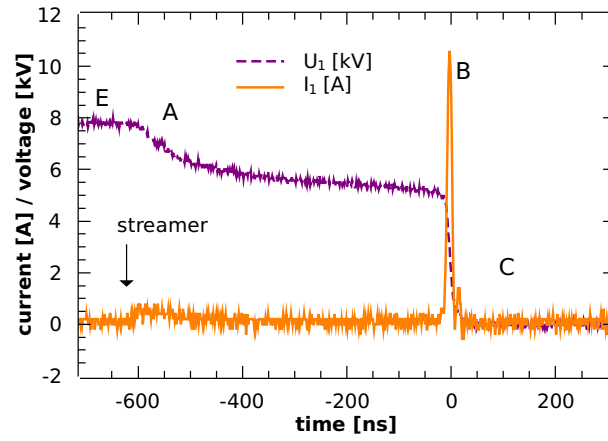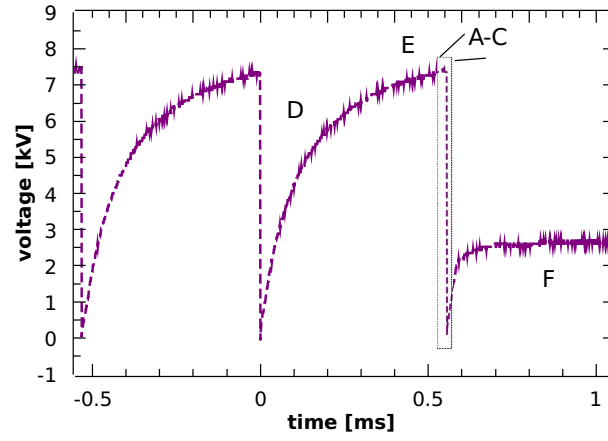**Figure 1.** Simplified scheme of the experimental set-up.

Figure 2. Photograph of TS in positive needle–plane gap of 6 mm, f=1.2 kHz, I_{max}=4 A, U_{TS}=7.5 kV, R=3.5 MΩ, exposure 0.25 s, ISO 200, aperture f/4.8.

a)

b)

Figure 3. Typical waveforms of transient spark in a) ns time scale, b) ms time scale, R=6.5 MΩ, f≈2 kHz, r=0 Ω, C=43±4 pF, $d = 5$ mm.
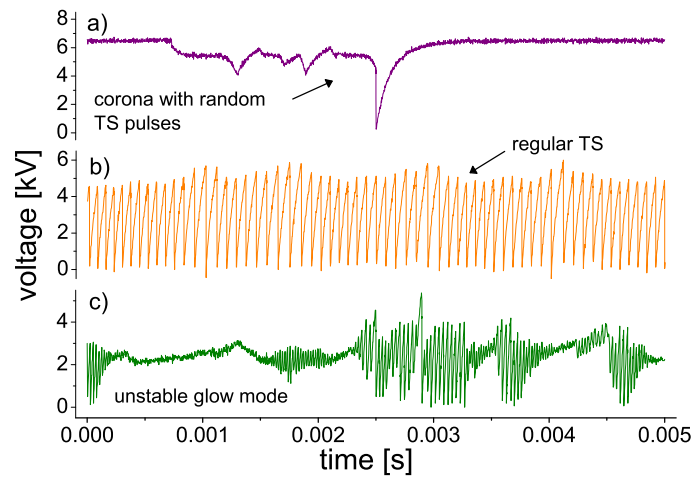
Figure 4. Voltage waveforms of different discharge regimes: a) the first random TS pulses, b) regular TS, c) unstable glow regime.
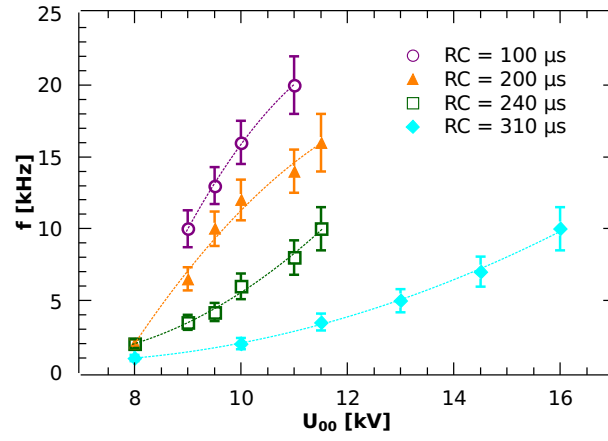
Figure 5. The dependence of f on the onset voltage U_{00} for several RC values, $r=0\,\Omega$, $d = 5\,\text{mm}$.
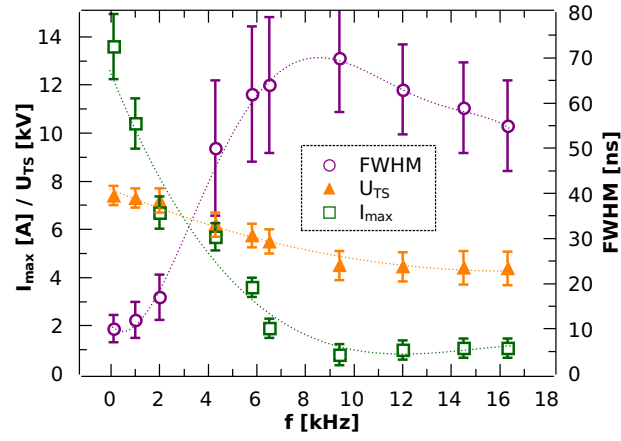
Figure 6. The dependence of peak current (I_{max}), breakdown voltage U_{TS} and FWHM of current pulses on f, $C = 32 \pm 4\,\text{pF}$, $R = 6.6\,\text{M}\Omega$, $r = 0\,\Omega$, $d = 5\,\text{mm}$.
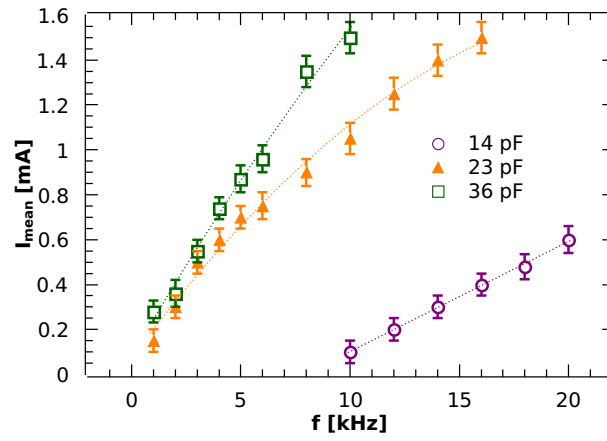
Figure 7. The dependence of mean discharge current I_{mean} on f, $R = 6.6\,\mathrm{M\Omega}$, $r = 0\,\Omega$, different values of C.
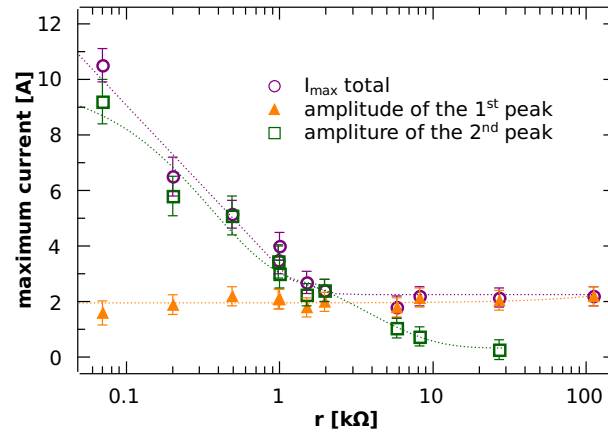
Figure 8. The influence of separating r on the amplitude of TS current pulse, and its two components, $R=9.84\,\text{M}\Omega$, $f\approx1.1\,\text{kHz}$, $C=43\pm4\,\text{pF}$.
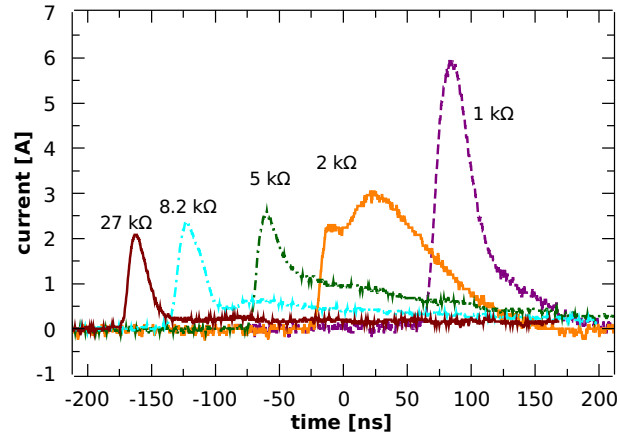
Figure 9. The influence of separating r on the shape of TS current pulses, R=9.84 MΩ, f≈1.1 kHz, C=43±4 pF.
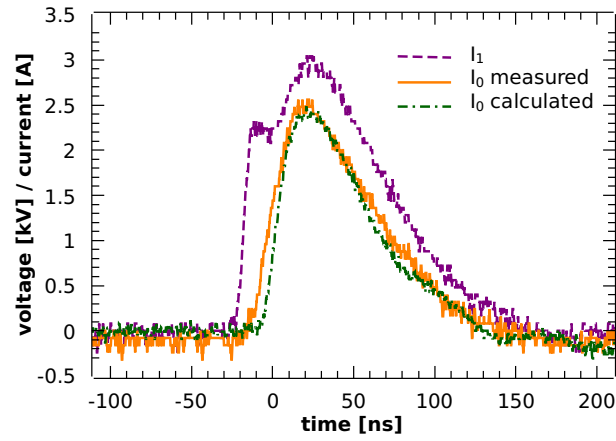
Figure 10. Comparison of I_0 measured by the current probe with I_0 calculated from U_0 and U_1, $r=2\,\text{k}\Omega$, $C=43\pm4\,\text{pF}$, $C_1^{'}=7\pm1\,\text{pF}$.
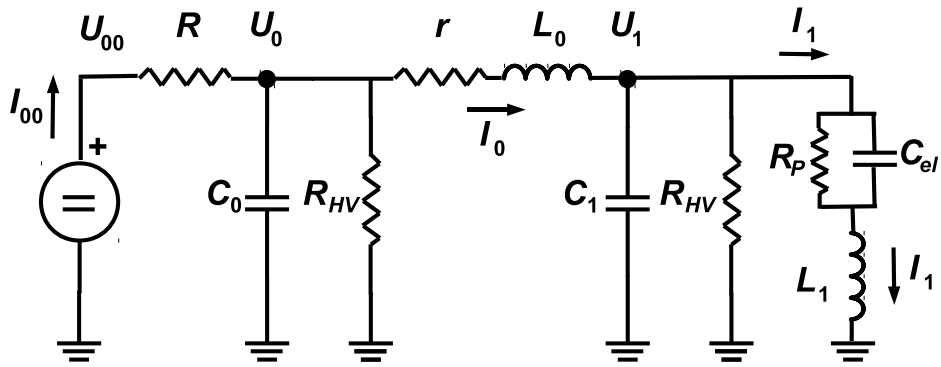
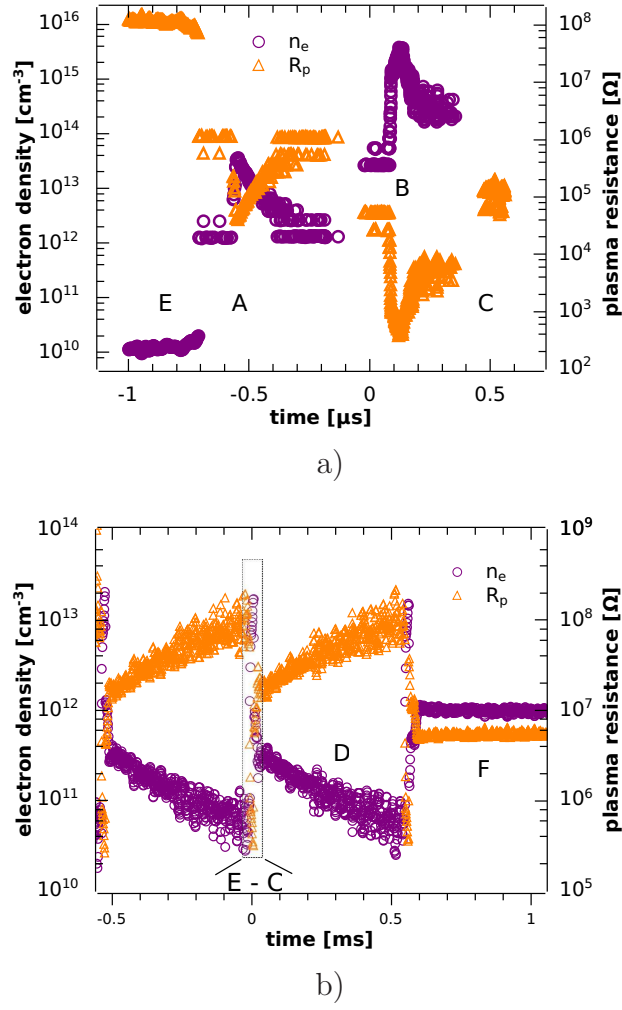**Figure 11.** A simplified electric circuit representation of TS.

Figure 12. Calculated electron density and plasma resistance during a TS pulse in a) μs time scale, b) ms time scale, r=0.9 kΩ, f≈2 kHz, C=32±4 pF.
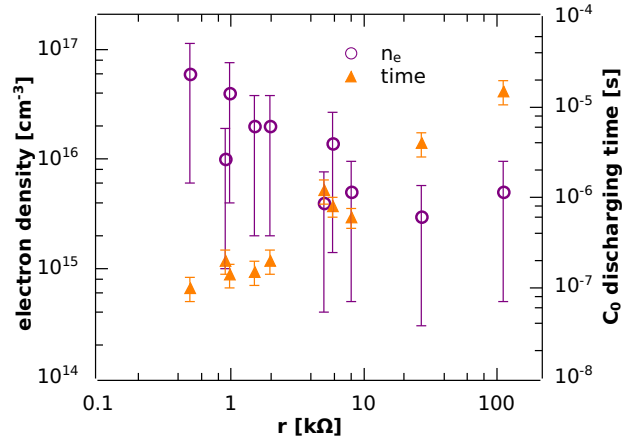
Figure 13. Dependence of maximum electron density and C_0 discharging time on r, R=9.84 MΩ, f≈2 kHz, C_0=37±3 pF, C_1=7±1 pF.

TRANSIENT SPARK – DC DRIVEN NANOSECOND PULSED DISCHARGE IN ATMOSPHERIC AIR

Mário Janda[1], Adriana Niklová[1], Viktor Martišovitš[1], Zdenko Machala[1]

[1]*Division of Environmental Physics*
Faculty of Mathematics, Physics and Informatics
Comenius University, Mlynska dolina F2
84248 Bratislava, Slovakia
E-mail: janda@fmph.uniba.sk

We introduce a DC-driven pulsed discharge named transient spark (TS): a repetitive streamer-to-spark transition discharge with short spark duration (~10-100 ns), based on charging and discharging of internal capacity C of the reactor with repetition frequency $f \approx$ 1-10 kHz. TS generates very reactive non-equilibrium air plasma and is applicable for flue gas cleaning, bio-decontamination or other applications, since it can be maintained at relatively low energy conditions (0.1-1 mJ/pulse). Streamer-to-spark transition is governed by the increase of the gas temperature T_g in the plasma channel. Initial T_g at the beginning of the streamer is ~300 K, though it increases with frequency up to ~450 K at 10 kHz. The transition to spark occurs at ~1000 K. This heating accelerates with increasing f, leading to a decrease of the average streamer-to-spark transition time from a few μs to less than 100 ns.

1. Introduction

Atmospheric pressure plasmas in air generated by electrical discharges present considerable interest for a wide range of environmental, bio-medical and industrial applications, such as air pollution control, waste water cleaning, bio-decontamination and sterilization, or material and surface treatment [1-5]. New types of discharges are therefore still being developed and studied, with a focus on efficiency, power requirements, stability, reliability and simplicity [6].

A novel type of transition discharge in air at atmospheric pressure named transient spark (TS) is presented here. TS is a filamentary streamer-to-spark transition discharge initiated by a streamer, which transforms to a short (~10-100 ns) high current (~1-10 A) spark pulse due to the discharging of the internal capacity C of the reactor. TS is based on charging and discharging of C and a repetition frequency of this process from 1 to 20 kHz can be achieved [7].

We observed significant differences between two modes of TS with small and high repetition frequencies [8], studied by time-integrated optical emission spectroscopy. In order to understand the fundamental phenomena related to the evolution of TS and its changes due to increasing repetition frequency, we employed in this study a photomultiplier tube with fast 2.2 ns rise time and appropriate narrow band optical filters, as well as a 2-m monochromator coupled with ICCD camera with 2 ns gate, in order to monitor time evolution of the emission of excited species and of the temperature.

2. Experimental set-up

Experiments were carried out at room temperature in atmospheric pressure air with a radial flow of about 20 cm/s. The distance between stainless steel needle electrode and planar copper electrode (point-to-plane configuration) was 4 mm. A DC High Voltage (HV) power supply connected via a series resistor ($R = 6.56$-9.84 MΩ) limiting the total current was used to generate a positive TS discharge. The discharge voltage was measured by a high voltage probe Tektronix P6015A and the discharge current was measured on a 50 Ω or 1 Ω resistor shunt. The 1 Ω resistor shunt was used when we focused on TS current pulse itself, whereas the 50 Ω resistor shunt was used to measure current from the streamer. Both voltage and current signals where recorded by a 200 MHz digitizing oscilloscope Tektronix TDS2024.

The emission spectra were obtained using a 2-m monochromator Carl Zeiss Jena PGS2 covering UV and VIS (200-800 nm) and providing spectral resolution of 0.05 nm, cuopled with an intensified CCD camera (Andor Istar). The iCCD camera was triggered by a home-made generator of 5 V rectangular pulses with rise time less than 5 ns. This generator was triggered directly by the current signal, causing

an additional delay of less than 10 ns. This delay, plus the delay caused by the transmission of the signal by BNC cables, was compensated by using 10 m long optical cable (Ocean Optics P400-10-UV-VIS), so that we could see the whole emission profile.

For time-resolved optical emission measurements, a photomultiplier tube (PMT) module with a 2.2-ns rise time (Hamamatsu H955) was also used in place of the monochromator. Its signal was recorded using the oscilloscope. The PMT was triggered by the emission signal itself. Whenever it was necessary to isolate a specific spectral transition for PMT measurements, a band pass interference filter, e.g. Melles Griot 03 FIU127 for the N_2(C-B 0-0) transition, was inserted into the optical path. The experimental set-up is depicted in Fig. 1.
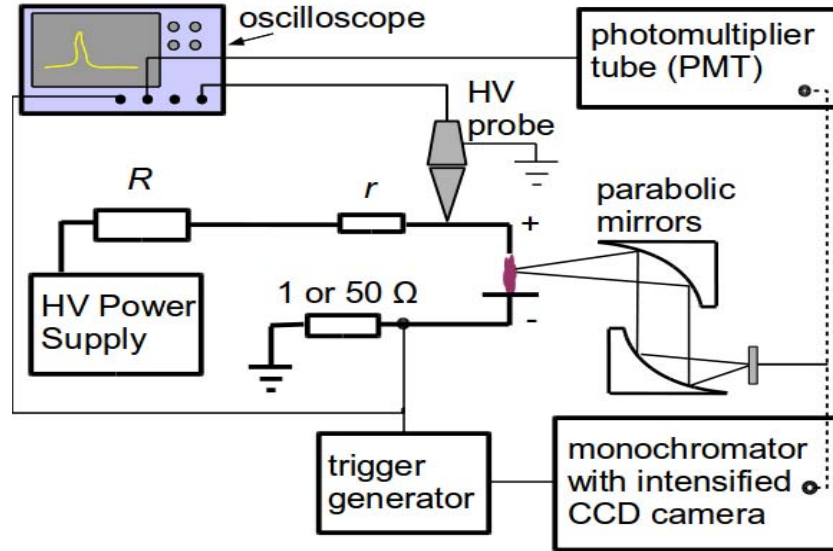

Fig. 1. Schematic of the experimental set-up, HV - high voltage, R, r - resistors.

3. Results and Discussion

When the high voltage U_{00} applied to the stressed electrode is progressively increased, we first observe a streamer corona. When the breakdown voltage is reached, a transition to TS occurs at the discharge voltage U_{TS}. The typical current and voltage waveforms are shown in Fig. 2a. During the high current phase the voltage drops to zero due to the resistive fall on the ballast resistance R. Then, during the quenched phase, the system capacity C (composed of the internal capacity of the electrodes, the capacity of the HV cable and of the HV probe) is recharged by a growing potential on the stressed electrode. For typical R and C, the repetition frequency f of this process is in the order of several kHz and grows with increasing U_{00} (Fig. 2b). This is accompanied by changes of TS properties. With increasing f, current pulses get smaller and broader (Fig. 3a).
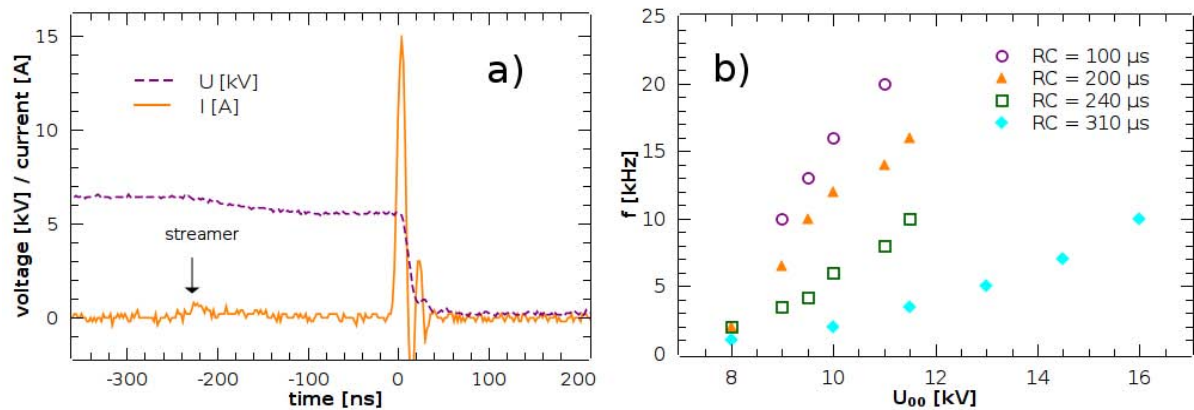

Fig. 2a. Typical TS current and voltage waveform, $f \sim 1$ kHz, $R = 6.6$ MΩ , $C \approx 26$ pF.
Fig. 2b. The dependence of TS repetition frequency on the onset voltage U_{00}.
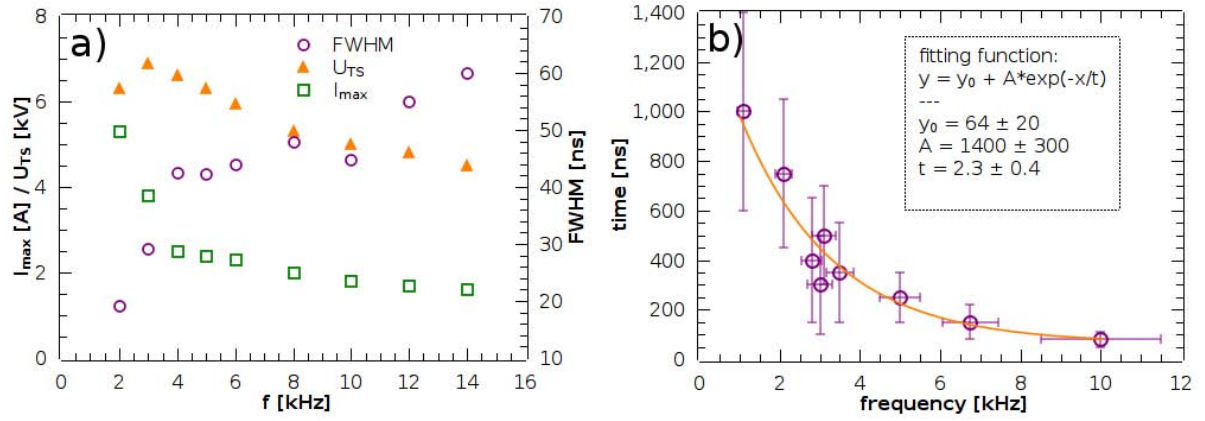
Fig. 3. Dependence of TS properties on f: a) peak current I_{max}, full width at half maximum FWHM of current pulses and breakdown voltage U_{TS}, b) streamer-to-spark transition time, $R = 6.6\,M\Omega$, $C \approx 26\,pF$.
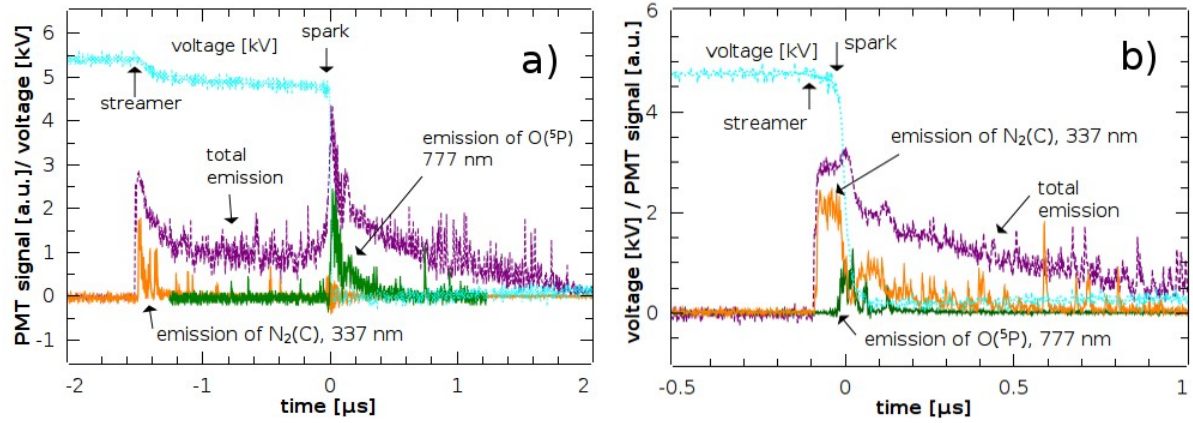

Fig. 4. Typical PMT emission profiles of TS at 2.5 kHz (a) and 6 kHz (b), $R = 6.6\,M\Omega$, $C \approx 26\,pF$.

It is interesting, that U_{TS} also depends on f (Fig. 3a). The decrease of U_{TS} with f was preliminary explained by the increasing gas temperature T_g, resulting in a decreasing gas density N. Since a certain threshold, the reduced electric field E/N is sufficient to initiate the TS pulse, E and thus also U_{TS} may be lowered [5]. Another reason may be memory effects – the gap remains pre-ionized by previous TS pulses as f increases [7]. Changes of streamer to spark transition time were also observed (Fig. 3b). At lower frequencies (< 2 kHz), the delay between streamer and spark formation is very random and it can vary from several μs to a few hundred ns. As f increases, the average delay time shortens and it becomes more regular.

Significant differences between lower and higher frequency regimes of TS were also observed in time-integrated emission spectra in VIS region. At low frequencies (<3 kHz), the emission of O, N and N^+ atomic lines dominated in the spectra, whereas at higher frequencies these atomic lines almost disappeared and N_2 1st positive system was much stronger. In UV region, N_2 2nd positive system dominated at all frequencies, but its relative intensity compared to atomic lines in VIS region also increased significantly with f. In order to understand this problem, we measured the time evolution of the emission from the strongest atomic line, O(^{5}P) at 777 nm, and from 0-0 band of N_2 2nd positive system at 337 nm by PMT with appropriate interference filters. Figures 4 a) and b) show typical emission profiles at these frequencies, plus the total emission profile at 2.5 and 6 kHz, respectively.

At lower frequencies, we can clearly see two peaks of total emission. The first one is produced by the streamer, whereas the second one corresponds to the short spark. It is obvious, that N_2(C) species are produced mainly during the streamer phase and O(^{5}P) species during the spark phase. The emission profiles also reflect the shortening of the streamer-to-spark delay time with increasing f. The two emission peaks therefore approach to each other and it is difficult to distinguish them at higher f.
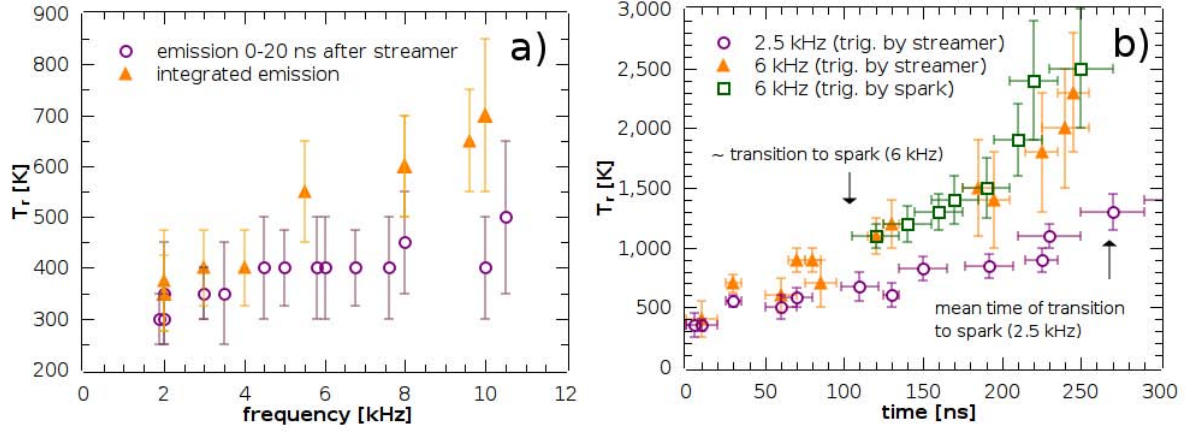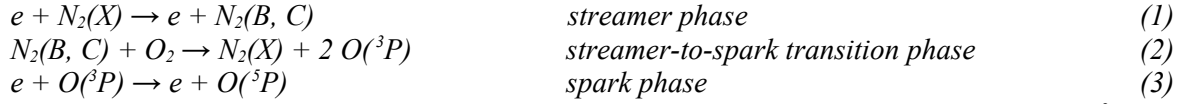
Fig. 5. The rotational temperature T_r of $N_2(C)$ as function of f (a) and time evolution of T_r (b).

The total emission from $N_2(C)$, obtained as an integral of PMT profiles, does not change significantly with f. The reason may be that $N_2(C)$ are mostly produced by collisions of energetic electrons with $N_2(X)$ during the streamer phase of TS and the properties of streamers (E/N, density of electrons n_e) do not change significantly with increasing f. On the other side, the total emission of $O(^5P)$ decreases with f quite significantly. This can be explained by changes of the spark pulse phase of TS with f (Fig. 3a), since $O(^5P)$ are mostly produced during this period. Another possible explanation might be a more complicated mechanism of $O(^5P)$ generation. We suggest the following three step mechanism:

$e + N_2(X) \rightarrow e + N_2(B, C)$ *streamer phase*   (1)
$N_2(B, C) + O_2 \rightarrow N_2(X) + 2 O(^3P)$ *streamer-to-spark transition phase*   (2)
$e + O(^3P) \rightarrow e + O(^5P)$ *spark phase*   (3)

As the streamer-to-spark transition phase shortens with the growing f, less and less $O(^3P)$ atoms accumulate for the production of $O(^5P)$ during the high current phase by the reaction (3). This does not necessarily mean that the production of $O(^3P)$ decreases significantly with f, it could be just shifted to later phase of TS, after the high current phase. Here, E/N is not strong enough for electrons to gain energy needed to excite $O(^3P)$ to $O(^5P)$. However, we cannot exclude other reactions that could be responsible for the production of $O(^5P)$, e. g. reactions including some metastable species such as $N_2(A)$, $NO(A)$, $O_2(a)$, $O_2(b)$ or $O(^1D)$.

As can be seen in Fig. 4, PMT profiles are quite noisy. The reason is that these emission profiles are from single TS pulses. It was not useful to acquire emission profiles by accumulation of many pulses due to a random character of streamer-to-spark transition. Data from iCCD camera, where the accumulation was necessary, were therefore used mainly for the calculation of rotational temperature T_r of $N_2(C)$ species, obtained by fitting the experimental spectra of N_2 2nd positive system with the simulated ones (using Specair program [9]). We further assumed that in our plasma $T_r \approx T_g$.

Let us explain the reason of the U_{TS} decrease with increasing f from the measured T_r. At the first moment it seems that T_r^{init} calculated from the initial 0-20 ns from the beginning of the emission induced by streamer increases only slightly with f, from about 300 to 450 K, compared to T_r^{total} calculated from time integrated emission of TS (typical integration time 300 µs − 3 ms), which increased to around 700 K (Fig. 5a). However, even this small T_r increase to 450 K is enough to keep an average E/N in the gap about 70 Td when the gap potential at the breakdown voltage U_{TS} decreases from about 7 kV to 4.5 kV (Fig. 3a). The value of T_r^{total} we previously used to describe the increase of T_g with increasing f has actually no physical meaning. To explain it, let us first look at the dependence of T_r on the time from the beginning of the streamer (Fig. 5b).

At both f=2.5 kHz and 6 kHz we observed approximately linear increase of T_r with time, from initial ~300 and ~400 K, respectively. This heating is faster at 6 kHz, but in both cases a streamer-to-spark transition occurs when T_r ~1000 K. We thus suppose that the increase of T_g is a dominant mechanism responsible for the streamer-to-spark transition, leading to the increase of E/N in the streamer plasma column from about 60-70 Td to about ~150-170 Td due to the decreasing N, under an assumption of the constant pressure.

The reason why the delay between the streamer and spark phase shortens with f can be explained by a faster growth of T_g with increasing f. However, this will require further research and deeper analysis, including kinetic modeling to explain why the growth of T_r accelerates with f.

During the spark phase, T_r increases even faster and can reach at least ~2500 K (Fig. 5b), but we were not able to measure it longer than ~250 ns from the beginning of the streamer, because the 2nd N_2 positive signal became too week.

Finally, relatively significant increase of T_r^{total} with f can be also explained by a faster growth of T_r with time at higher discharge frequencies. Despite the fact that the whole $N_2(C)$ emission profile contributes to T_r^{total}, we suppose that initial ~100 ns with the strongest intensity dominate. Thus, T_r^{total} represents only something like average T_r during these ~100 ns after the beginning of the streamer emission. At 2.5 kHz, T_r increases to about 600 K during these period, whereas at 6 kHz it is already ~1000 K, which gives T_r^{total} around 400 K and 600 K, respectively. In fact, significant changes of T_r during these ~100 ns also explains large errors of T_r^{total}, despite the signal was strong enough during the measurement of time-integrated spectra. In time-resolved measurements with iCCD gate open for up to 20 ns, the major sources of uncertainties were a weak signal and a random character of TS.

4. Conclusions

We investigated electrical characteristics and time-resolved emission profiles of a DC-supplied periodic streamer-to spark transition discharge in atmospheric air, called transient spark (TS). Thanks to the small internal capacity of the discharge chamber and a limiting series resistor, TS is characterized by the very short spark pulse duration (~10-100 ns) with peak current 1-10 A. TS can be maintained at low energy conditions (0.1-1 mJ/pulse) and generated plasma cannot therefore reach LTE conditions, though the current pulse can lead to temporary increase of temperature to ~2500 K. The global temperature however remains relatively low, since even at repetition frequencies above 10 kHz, each streamer-to-spark process starts at ~450 K.

Subsequent increase of temperature to ~1000 K, accompanied by the increase of the reduced electric field strength inside the plasma channel, governs the streamer-to-spark transition. Shortening of an average streamer-to-spark transition time with increasing TS frequency can be explained by an acceleration of temperature growth. The reason for this acceleration will require further research.

More research is also needed to explain chemical effects of TS. Emission profiles show that streamer is responsible for significant part of the total emission and for almost all emission of N_2 2nd positive system. This proves the importance of streamer in plasma chemistry, but it does not explain why TS was demonstrated more efficient for bio-decontamination than streamer corona. [5] We suppose that during the initial phase of the spark pulse, the strong chemical effect can be maintained thanks to the combination of a relatively strong reduced electric field (>100 Td) and a high electron density.

5. References

[1] Civitano L 1993 Non-Thermal Plasma Techniques for Pollution Control, eds. Penetrante B and Schultheis S E (Springer, New York) NATO Series, Vol. 1, p. 103.
[2] Joshi A A, Locke B R, Arce P, Finney W C 1995 *Journal of Hazardous Materials* **41** 3.
[3] Cernak M et al. 2004 *Contrib. Plasma Phys.* **44** 492.
[4] Pawlat J et al. 2005 *Acta Phys. Slovaca* **55** 479.
[5] Machala Z et al. 2007 *J. Mol. Spectrosc.* **243** 194.
[6] Pai D et al. 2008 *IEEE Trans. Plasma Sci.* **36** 974.
[7] Janda M et al. 2010 *Acta Physica Universitatis Comenianae* **L-LI** 85-93.
[8] Machala Z et al. 2009 *Eur. Phys. J. D* **54** 195.
[9] Laux C O 2002 Radiation and Nonequilibrium Collisional-Radiative Models, von Karman Institute for Fluid Dynamics, Lecture Series 2002-07, Rhode Saint-Genese, Belgium